FACULTY OF MEDICINE AND HEALTH SCIENCES

Investigating the therapeutic potential of Tonabersat for the treatment of GB using the F98 GB rat model

ketelaere Ellen
Student number: 01802733

Supervisor(s): Prof. Dr. Deblaere Karel, Dr. De Meulenaere Valerie, Drs. Zoteva Velislava

A dissertation submitted to Ghent University in partial fulfillment of the requirements for the degree Master of Science in the Biomedical Sciences

Department of Diagnostic Sciences, Ghent University Hospital

Academic year: 2022 – 2023

GHENT UNIVERSITY

Preface

This thesis marks the end of five years of studying Biomedical Sciences at Ghent University. I would not have accomplished this without the help of people I would like to thank.

First, I want to thank my promotor Prof. Dr. Karel Deblaere for the opportunity to work in this research group on this interesting topic. I also want to thank my copromotor Dr. Valerie De Meulenaere for the guidance and the feedback during this dissertation. But in particular, I want to thank my mentor Ir. Vivi Zoteva for teaching me all the laboratory techniques, for the guidance during the experiment, for trusting me with the care of her beloved rats and for all the feedback during the writing of this dissertation. I also want to express my gratitude to Prof. Dr. Christian Vanhove and Dr. Benedicte Descamps for the warm welcome in the Infinity lab and the help when technical issues occurred.

Secondly, I'm very thankful for having a great lab partner by my side. Therefore, I want to thank Amber Meskens for all the support during this experiment, for all the days and weekends spend together in the lab, but especially for the talks and her friendship.

Lastly, my special thanks go to my friends from biomedical sciences, with who I had a lot of pleasure during these five years of studying. In addition, I want to thank my mother for always believing in me and for having my back during the difficult moments. Last but not least, I want to thank my boyfriend Jelle for encouraging me and supporting me during the five past years.

Ellen ketelaere

May, 2023

Table of Contents

Summary

The 5-year survival rate of glioblastoma (GB) is 5%, despite the multimodal standard medical treatment (ST) consisting of surgical resection, followed by radiotherapy (RT) and concurrent and adjuvant temozolomide (TMZ) chemotherapy. This poor prognosis is partly due to the development of overall resistance to the cytotoxic effects of the therapy and tumour recurrence. Especially connexin 43, a building block of gap junctions, might be involved in the formation of a resistant cellular network in GB through the formation of microtube-associated gap junctions (i.e., tumour microtubes). Therefore, new therapeutic strategies inhibiting these tumour microtubes are researched. This preclinical study investigates the adjuvant therapeutic potential of Tonabersat, a gap junction inhibitor, using the F98 GB rat model. After intracranial inoculation of female Fischer rats with 5.000 F98 tumour cells, contrast-enhanced T1 weighted (CE T1w) magnetic resonance imaging (MRI) is used to confirm GB growth. Subsequently, the rats were randomized in 4 groups, i.e. a ST (fractionated RT and TMZ chemotherapy) control group, a ST and Tonabersat group, a fractionated RT and Tonabersat group and a TMZ chemotherapy and Tonabersat group. To follow-up GB growth, CE T1w MRI sequences were performed at fixed time-points. Kaplan-Meijer survival analysis demonstrated a significant difference in survival time between the control group and ST and Tonabersat group. Comparison of geometric mean tumour volumes and tumour growth rates resulted in no significant difference between these treatment groups. Our results indicate a therapeutic potential of Tonabersat when added to the standard medical treatment.

Layman summary with societal impact

Almost half of the primary malignant brain tumours are GBs. The diagnosis of GB is a hard verdict for patients because GB is associated with a low survival rate and many clinical symptoms, including epileptic seizures and intracranial pressure. The current treatment strategy consists of surgical resection, radiotherapy and chemotherapy, but fails to significantly increase the survival rate due to the overall resistance to this therapy. Therefore, development of new therapies is necessary for GB. The results of this preclinical study using the F98 GB rat model show that Tonabersat may add value to the standard of care. In particular, the patient's life span after diagnosis could feasibly be prolonged by the addition of Tonabersat. On top of this, the results seem to indicate that omitting chemotherapy does not affect the survival time significantly. In the future, this could lead to a strategy consisting of a combination of radiotherapy and Tonabersat, which would be an advantage for the patient because the toxic side-effects of chemotherapy on the body (e.g. hair loss and nausea) could be cleared. The application of Tonabersat in humans showed no serious side-effects when evaluated in phase II clinical trials for migraine prevention. This may increase the patient's quality of life. Besides GB, Tonabersat might serve as a therapy for other cancer types (e.g. breast cancer and prostate cancer) where Cx43 seems to be involved in therapy resistance and tumour invasion.

1.Introduction

1.1. Brain microenvironment

The brain microenvironment consists of two main cell types, namely neurons and glial cells[1,2]. The glial cells are present in large numbers and occupy about half the volume of the brain[1]. Recent studies have shown that the glia/neuron ratio is approximately equal to 1[3]. In the central nervous system (CNS), the three types of glial cells are astrocytes, oligodendrocytes and microglial cells.

Neurons are responsible for the rapid communication via electrical and chemical signals in the CNS. This communication occurs through synapses, which allow for signals to be transmitted between neurons or from neurons to other cells, such as muscle cells[4].

It was long thought that glial cells had only a supportive function in the neural tissue[2]. Nowadays it is shown that these cells play more active and important roles in brain development and brain function[2]. Astrocytes are the most abundant glial cells and are characterised by their star-shaped appearance[2]. These astrocytes have multiple functions in the CNS, more specifically maintaining homeostasis of the brain, regulating synaptic transmission, protecting neurons against toxic compounds and providing energy and substrates to neurons. Moreover, astrocytes can contact blood vessels and control the maintenance of the blood-brain barrier (BBB)[1]. In addition, astrocytes play a role in secretion or absorption of excess neurotransmitters present in the brain. Oligodendrocytes are responsible for the formation of the myelin sheath around the axons, allowing rapid conduction of electrical signals in the brain[1]. Lastly, the microglia cells are macrophage-like cells, which act as phagocytes. They are referred to as the immune cells of the CNS, protecting the brain from injury and infection[1,2].

Of note, glial cells can also be associated with certain pathologies, including Alexander disease and Multiple Sclerosis[2]. In addition to these diseases, the majority of malignant brain tumours is derived from glial cells or their progenitors[1].

1.2. Blood-brain barrier

The BBB is a heavily restrictive barrier in the brain's capillaries and venules, that separates the brain from the circulatory system[2,5,6]. Tight regulation of the movement of molecules, ions and cells between the blood and the CNS is the main function of the BBB. This leads to an optimal control of the CNS homeostasis, which is necessary for proper neuronal functioning, and protection of the CNS from pathogens and disease[6]. This function comes about through the interaction of astrocytic endfeets, neurons, pericytes and microglia with the endothelial cells[5,6]. The formation of the BBB during embryonal development is regulated by pericytes. In addition, pericytes ensure that the BBB function is maintained during adulthood and aging[6].

The movement of molecules, ions and cells through the BBB is made possible by structural and transport components[7]. Tight junctions form the main barrier to macromolecules and most polar solutes[7]. Passive diffusion into the brain is possible if the molecules are lipid soluble and their molecular weight is less than 500 Da[8]. In addition to these tight junctions and passive movement, transporters are present at the BBB[6]. There are two main types of transporters expressed in the CNS: efflux transporters and nutrient transporters. Efflux transporters use ATP to transport their substrates up their concentration gradient, these are part of the ATP-binding cassette (ABC) transporters[6]. Nutrient transporters facilitate the movement of many essential polar nutrients, such as glucose and amino acids, down their concentration gradient. Large molecules, for example proteins and peptides, can enter the CNS by transcytosis[7]. This restrictive and tightly regulated nature of the BBB provides a difficulty for the delivery of drugs to the CNS[6]. Loss of these barrier properties is seen in many neurological diseases, including stroke, brain traumas and neurodegenerative disorders[6].

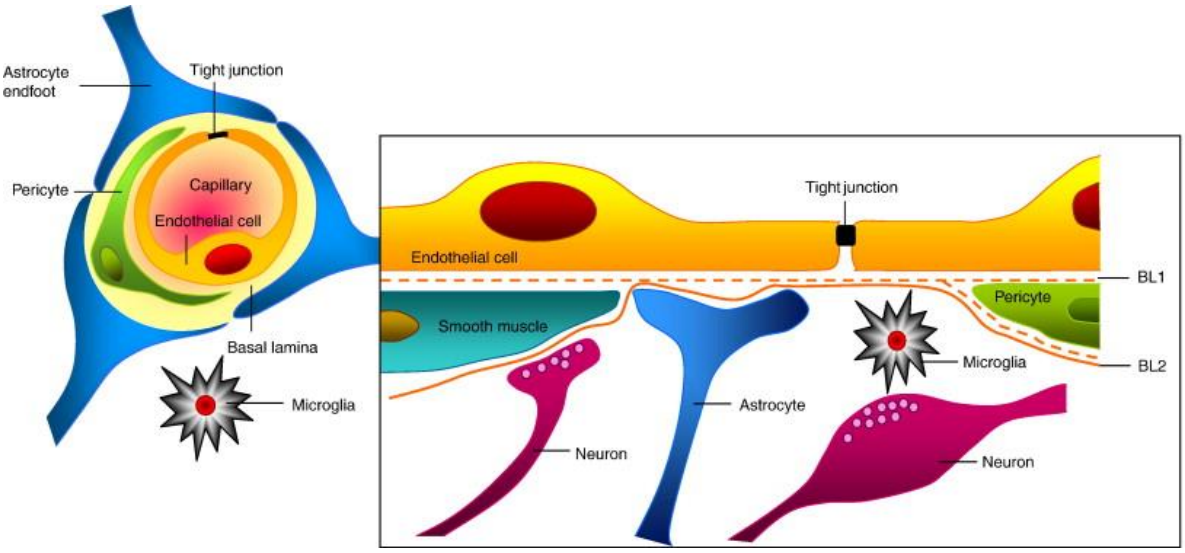

Figure 1: The BBB and its structural units[7].

1.3. Glioma

Gliomas account for almost 80% of all malignant primary brain tumours and are the most commonly occurring tumours of the CNS[9]. Diffuse gliomas are both the most common and malignant primary brain tumours in adults, characterised by a diffuse infiltration into the brain parenchyma and are prone to malignant progression[9,10]. Neural stem cells, glial progenitor cells or astrocytes are considered as the cellular origin of these malignant gliomas and transformation of these cells can promote gliomagenesis[11]. Gliomas form a heterogeneous group of tumours of the CNS, and are mostly observed in the cerebral hemispheres[12]. The World Health Organisation (WHO) categorized the gliomas into four histological grades (1-4) in 2017[13]. Grade 1 lesions are benign and show a slow proliferation[10]. Grade 2 tumours grow diffusely into the brain parenchyma and can form malignancies. Grade 3 tumours have a higher cellular density and contain a lot of cells which undergo mitosis. Lastly, grade 4 tumours are the most malignant, these are characterised by microvascular proliferation and necrosis[10]. Molecular features combined with histologic grading were incorporated into this classification system in 2016. In 2021, another update of this classification system was introduced, which included changes in CNS tumour taxonomy, CNS tumour nomenclature, gene and protein nomenclature for CNS tumour classification, CNS tumour grading (Arabic vs Roman numerals, grading within types, etc.), NOS (Not otherwise specified) and NEC (Not elsewhere classified) diagnoses, novel diagnostic technologies, integrated and layered diagnoses, newly recognized entities and revised nomenclature[14,15].

1.4. Glioblastoma

Glioblastoma (GB), also known as glioblastoma multiforme, is the most malignant glioma type and belongs to grade 4 of the WHO classification system[13]. Most GBs are located in the supratentorial compartment of the brain. GB can be classified in two types, primary and secondary. GBs arising from progression of WHO grade 2 diffuse gliomas are termed secondary, these occur in younger patients (<40 years old) and have a better prognosis[16,17]. In contrast, GB developing rapidly, without a known less malignant precursor lesion, are designated primary or *de novo* GBs and account for 90% of GBs[16,17].

45,6% of the primary malignant brain tumours are GBs[18]. The annual incidence of GB increases with age from 0,15 per 100.000 in children to the highest incidence of 15,03 per 100.000 in the 75-84 age group[18]. The risk factors of developing GB are poorly defined. Hereditary cancer syndromes, such as Li-Fraumeni syndrome and neurofibromatosis type 1 and 2, are sometimes associated with GB development. Exposure to radiation therapy at a younger age is the only known exogenous risk factor for GB[9,18]. Headache, increased intracranial pressure and the onset of epileptic seizures are known clinical symptoms of

GB[9,18,19]. The destructive effect of the tumours on the brain function often leads to cognitive and emotional deficits in patients[12].

1.4.1. Diagnosis

The diagnosis of GB is made based on symptoms, clinical examinations, and the use of imaging techniques. Standardly, GB is diagnosed with magnetic resonance imaging (MRI), typically a gadolinium (Gd)-enhanced T1-weighted MR sequence is used[20]. This is followed by a histopathological examination to confirm the diagnosis[9]. The histopathological characteristics of GB include necrosis and microvascular proliferation[18]. In addition, immunohistochemical markers such as glial fibrillary acidic protein (GFAP) expression, are used to ascertain the diagnosis[18].

1.4.2. Treatment

After diagnosis, an extensive therapy process is started. The current standard of care consists of maximal surgical resection, followed by radiotherapy and concurrent and adjuvant chemotherapy with temozolomide (TMZ)[21]. This is known as the Stupp protocol and has been the standard of care since 2005[22]. Radiotherapy is typically delivered in daily fractions of 2 Gy given five days per week for six weeks, so 30 fractions for a total of 60 Gy[21,22]. TMZ is an oral alkylating agent and methylation of DNA, leading to cell cycle arrest, is the major mechanism of action responsible for the cytotoxicity to malignant cells[22,23]. During radiotherapy, TMZ is given daily in a dose of 75mg/m² for six weeks. Afterwards, there are six maintenance cycles of TMZ, during these cycles the dose is increased to 150-200mg/m²/day for the first five days of a 28-day cycle[21]. Despite this extensive treatment approach, the survival rate is limited, with a median survival of approximately 15 months from the diagnosis[24]. Stupp et al. showed that the survival rate for radiotherapy treatment alone was approximately 12 months[22]. Addition of concurrent TMZ treatment leaded to a 2 month increase, resulting in an approximately 14 month survival rate. Five years after diagnosis only 5% of the patients survive and this 5-year survival rate even decreases to 2% in the 65+ age group[18]. The standard treatment has a limited efficacy due to the high rates of recurrence, overall resistance to therapy and neurological deterioration[25]. Another main characteristic of GB, besides the resistance to therapy, is the complex intra- and inter-tumour heterogeneity, which is also involved in the therapy failure[5].

1.5. Molecular markers

There are several molecular markers known to be clinically relevant and serve as diagnostic and prognostic marker for patients diagnosed with GB[24]. To confirm the diagnosis of GB, one of these molecular alterations needs to be present, namely: epidermal growth factor receptor (EGFR) amplification, telomerase reverse transcriptase (TERT) promotor mutation or concurrent gain of chromosome 7 and loss of chromosome 10 (+7/-10) (as shown in figure 2)[14].

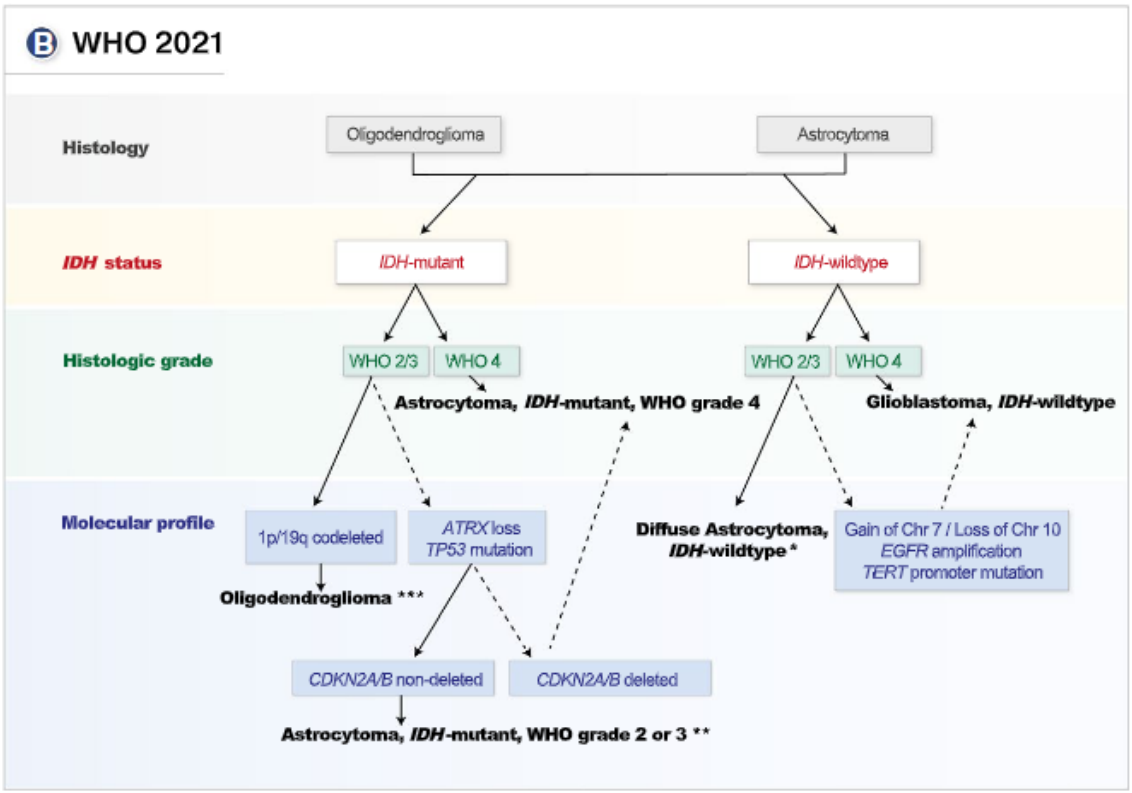

Figure 2: Classification of diffuse gliomas based on the 2021 edition of the WHO classification of CNS tumours. GB belongs to the astrocytoma and is considered an isocitrate dehydrogenase (IDH)-wildtype, grade 4 tumour. Molecular testing for gain of chromosome 7 and loss of chromosome 10 (+7/10), epidermal growth factor receptor (EGFR) amplification or telomerase reverse transcriptase (TERT) promotor mutations are required for GB[14].

1.5.1. EGFR amplification

Upon binding of ligands to the EGFR, processes like proliferation, differentiation and survival of cells are regulated[26]. Approximately 40% of all primary GBs carry amplification of the *EGFR* gene[24]. Downstream signaling pathways of this receptor result in tumour cell invasion, angiogenesis and proliferation[27]. Talasila et al. demonstrated that *EGFR* amplification promotes invasion and GB development independent of angiogenesis, while loss of EGFR activity leads to angiogenic tumour growth[27]. Half of all GBs overexpressing *EGFR* have a deletion in the extracellular ligand-binding domain of *EGFR* (EGFRvIII)[18]. Therefore, EGFRvIII is the most prominent mutated tyrosine kinase receptor in GB[28]. This deletion makes the receptor constitutively active and promotes a more invasive phenotype[28].

1.5.2. TERT – promotor mutation

TERT promotor mutations are present in approximately 70%-80% of primary GBs[24]. TERT is the catalytic subunit of the human telomerase complex, which regulates the length of the telomeric DNA at the ends of the chromosomes[24]. It counteracts physiological telomere shortening[29]. Mutations in the TERT promotor are often found in malignant tumours. This leads to an unlimited mitotic capacity of the tumour cells, due to inhibition of telomere shortening caused by telomerase activation. TERT promotor mutations are associated with a poor overall patients' survival[29].

1.5.3. +7/-10 chromosome copy number variation

Whole or partial loss of chromosome 10 and whole or partial gain/amplification of chromosome 7 are the most frequent genetic abnormalities in GB[30]. A gain of 7p is often detected in grade 4 tumours. *EGFR* is an oncogene located on 7p, thus a gain of 7p results in *EGFR* amplification[30]. The phosphatase and tensine homolog (*PTEN*) gene and deleted in malignant brain tumours 1 (*DMBT1*) gene, both tumour suppressor genes, are located on 10q[24,30]. Therefore, loss of 10q is associated with loss of tumour suppressor genes. Most patients with 7p amplification have a simultaneous loss of 10q. Therefore, Arslantas et al. suggest that

oncogenes present on chromosome 7 might have regulatory effects on tumour suppressor genes of chromosome 10[30].

1.5.4. *IDH1*-mutations

Since the update of the WHO classification in 2021, GB is considered as an Isocitrate Dehydrogenase (IDH) wildtype tumour[14]. Previously, *IDH1/2* gene mutations were an important molecular marker for secondary GB[31]. Mutations in *IDH1* tend to occur more frequently in younger patients and in patients with secondary GB. In these patients an increase in overall survival is seen[31].

1.5.5. *MGMT* promotor methylation

One of the most important therapeutic markers in GB is O^6-methylguanine-DNA methyltransferase (MGMT) promotor methylation[24]. The *MGMT* gene encodes a DNA repair protein. This protein transfers alkyl groups, which are produced by chemotherapeutic alkylating agents, from the O^6 position of guanine to its own molecule, which restores the DNA[28]. This *MGMT* function may be impaired by hypermethylation of its promotor, which results in gene silencing. Loss of MGMT-mediated repair may lead to DNA strand breaks, induced by for example TMZ, which eventually results in tumour cell death[28]. Therefore, MGMT promotor methylation is a predictive marker for the response to TMZ treatment[24]. Unfortunately, only 40% of GB patients has a MGMT promotor methylation and thus responds well to TMZ treatment[24].

1.5.6. Other molecular markers

The Vascular Endothelial Growth Factor (VEGF) may be overexpressed, resulting in neovascularization and angiogenesis[28]. Besides loss of the tumour suppressor genes *PTEN* and *DMBT1*, other tumour suppressor genes such as Tumour Protein 53 (*TP53*), Retinoblastoma 1 (*RB1*), Cyclin Dependent Kinase Inhibitor 2A (*CDKN2A*) and Alpha Thalassemia/mental Retardation syndrome X-linked (*ATRX*) might be mutated or deleted[24]. The p53 and Rb pathways can also be disrupted by mutations in genes encoding upstream regulators. For example, Cyclin-dependent kinase 4 (Cdk4), which is a repressor of Rb is often upregulated in GB by gene amplification[24].

1.6. Tumour microenvironment

In addition to cancer cells, the tumour microenvironment consists of a mixture of different non-cancerous cell types[32].

1.6.1. Tumour-associated macrophages (TAMs)

An essential part of the tumour microenvironment are tumour-associated macrophages (TAMs)[11]. On average 40 % of the GB tumour mass consists of TAMs that can arise from microglia-brain tissue-resident and bone marrow derived macrophages (BMDMs), recruited from the circulation[11,33]. In pathological conditions, such as BBB disruption in GB, monocytes extravasate and populate the inflamed brain tissue, where they give rise to BMDMs[33,34]. TAMs are located both intra- and peritumourally and are attracted by GB cells via the release of chemoattractant factors[11].The release of transforming growth factor beta (TGF-β) by TAMS induces the expression of metalloproteinase-9 (MMP9), leading to an increased cancer stem cell (CSC) invasiveness[33,35].

1.6.2. Dendritic cells (DCs)

Dendritic cells (DCs) are antigen-presenting cells (APCs) that stimulate T-cell responses[34]. DCs play a less important role in the brain because microglia are the predominant APCs. DCs are not present within the brain parenchyma in healthy conditions[36]. But, in GB, DCs are being recruited to the brain via chemokines (e.g. CCL5) secreted by the tumour microenvironment and NK cells[36]. The microenvironment is able to induce a regulatory DC phenotype, which activate regulatory T-cells and downregulate the recruitment of $CD8^+$ effector T-cells, leading to an immunosuppressive environment[11,36]. DC vaccines are being researched to stimulate T-cell responses to the tumour[34].

1.6.3. Neutrophils

Neutrophils are attracted via macrophage migration inhibitory factor (MIF), C-X-C motif chemokine ligand 8 (CXCL8) and interleukin 8 (IL-8) to the tumour microenvironment and accumulate there[36]. Neutrophils facilitate tumour initiation, proliferation and dissemination[11]. In addition, they induce angiogenesis, attenuate the immune system and facilitate the extravasation of tumour cells. Moreover, neutrophils can induce an expansion of the glioma stem cell pool, resulting in tumour progression[34]. Therefore, neutrophils are negatively associated with the prognosis of GB patients[36].

1.6.4. Lymphoid cells

T-cells, B-cells and NK cells are the lymphoid cells of the immune system[34]. Cytotoxic T-cells, $CD4^+$ T helper cells and Tregs are the major tumour-infiltrating lymphocytes[11]. The tumour microenvironment of GB leads to T-cell impairment: exhaustion of T-cells, reduced effector functions, and increased surface expression of co-inhibitory immune checkpoints[11]. Regulatory B-cells are present in the tumour microenvironment and overexpress immunosuppressive molecules such as programmed death ligand 1 (PD-L1) and Cluster of Differentiation 155 (CD155) in addition to producing IL-10 and TGF-β[36]. NK cells have been found to infiltrate the tumour microenvironment in GB[36]. NK cells secrete cytokines to control tumour growth. However, GB cells can express unique major histocompatibility complex class I (MHC-1) molecules, resulting in a suppression of the antitumour functionality of NK cells[36].

1.6.5. Reactive astrocytes

The presence of tumour-associated astrocytes is an essential component of glioma[11]. Astrocytes can influence GB cells by performing immunological functions and becoming activated[11]. Astrocytes undergo morphological and functional changes under pathological conditions[11,32]. This is called astrogliosis and results in reactive astrocytes. In GB, reactive astrocytes arise when astrocytes contact tumour cells[19]. The characteristics of reactive astrocytes are hypertrophy, activation of cell proliferation and upregulation of intermediate filaments composed of nestin, vimentin and fibrillary acidic protein (GFAP)[19]. In addition, they express metalloproteinase-2 (MMP2) and secrete stromal cell-derived factor-1 (SDF1), resulting in parenchymal infiltration and uncontrolled proliferation of glioma cells, respectively[19].

1.6.6. Tumour niches

The tumour microenvironment can be compartmentalized in different tumour niches[35]. These niches contain several stromal cells, such as microglia, astrocytes, pericytes, fibroblasts and endothelial cells, but also GB stem-cell like populations[32,35]. In GB at least three tumour niches exist: the perivascular, the invasive and the hypoxic niche[35,37]. CSCs are in direct contact with the endothelium of the abnormal angiogenic vasculature in the perivascular tumour niche. In the invasive niche perivascular growth of single invasive tumour cells occur, resulting in detachment of astrocyte end-feet and pericyte dissociation, enabling migration into the brain parenchyma[35,38]. In the hypoxic tumour niche the blood vessels are non-functional or regressed, which results in necrotic areas[35].

1.6.7. Cancer stem cells (CSCs)

CSCs are multipotent and appear to be involved in tumour initiation and self-renewal capacity[5]. Another function of the CSCs is recruitment of immunosuppressive cells into the tumour microenvironment. The extracellular matrix (ECM) supports CSCs and contributes to tumour progression and chemoresistance[5,36]. These CSCs are anchored in the perivascular niche by the ECM, which secretes growth factors that lead to CSCs proliferation[32].

1.6.8. Communication in the tumour microenvironment

GB cells closely interact with their direct microenvironment. The tumour cells communicate with the surrounding normal brain cells in a bidirectional manner, leading to an immunosuppressive microenvironment that allows cancer progression[11]. Intercellular

communication between cells from the tumour microenvironment is essential for proliferation and metastasis. These interactions can be mediated via direct exchanges, for example via extracellular vesicles, gap junctions, ion channels and transporters, or via soluble factors, such as neurotransmitters, cytokines/chemokines and growth factors[11]. The tumour cells can affect surrounding cells by secreting several factors[32]. For example, proangiogenic cytokines and chemokines can induce proliferation and rearrangement of endothelial cells into blood vessels that integrate in the tumour. In addition, the high expression of VEGF leads to angiogenesis in the GB tumour[5]. In GB, this increase in vascularisation, which contributes to leakiness of blood vessels, causes inflammation and physical distortion, which can result in a compromised BBB[36]. Disruption of the BBB enables the entrance of immune cells, which can activate the astrocytes and promote neuroinflammation[11].

1.6.9. The extracellular matrix (ECM)

The ECM is composed of hyaluronic acid, proteoglycans, and associated proteins, these are overexpressed by tumour and tumour associated cells during tumour development[32]. This results in an increased stiffness of the tumour-associated ECM[36]. The dense microenvironment leads to metabolic stress and hypoxia, which is a characteristic of GB[5,36]. Hypoxia induces a metabolic adaptation in the tumour cells, resulting in a selection and survival of the most aggressive cancer cells[39].

1.6.10. Hypoxia

Not only specific cell types but also specific conditions can contribute to the tumour microenvironment[5]. Hypoxia is the consequence of the fact that not all tumour cells can be supplied with blood and oxygen due to the rapid uncontrolled tumour growth and has been associated with invasion, metastasis and tumour recurrence[39].The low tumour oxygenation enhances CSC maintenance, chemoresistance and supports tumour growth, resulting in a more aggressive type of tumour. In addition, the hypoxic microenvironment can induce epithelial-to-mesenchymal transition (EMT)[11]. The new-formed mesenchymal cells can interact with the non-neoplastic cells (e.g. immune cells), altering their activities[11].

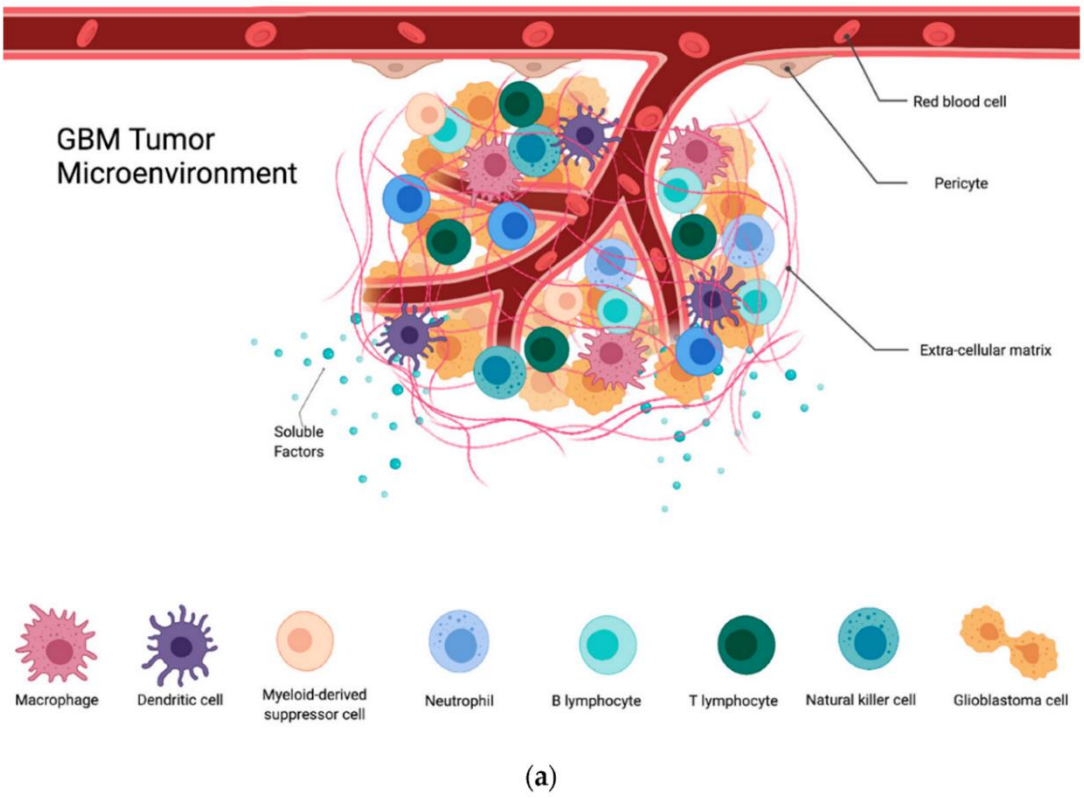

Figure 3: Overview of the different cell contributing to the GB tumour microenvironment[t36].

1.7. Connexins

Connexins are transmembrane proteins[40]. These connexins can oligomerize into a hexameric hemichannel, also called a connexon[41]. These channels connect a cell's cytoplasm to the extracellular space, allowing exchange of small molecules and ions, such as glutamate and calcium[40-42]. This communication pathway is important for autocrine and paracrine signalling[43]. When such a hemichannel docks to another hemichannel, located on an adjacent cell, a functional cell-to-cell channel, called gap junction (GJ), is formed (as shown in figure 3)[41]. GJs allow the transport of molecules between the cytosols of two connected cells facilitating bidirectional cytosolic exchange of ions, metabolites and secondary messengers[41,44]. In humans, there are 21 known connexins[41,43]. They are named after their predicted molecular mass, e.g. connexin 43 (Cx43) has a molecular mass of ~43kDa[41]. From these 21 connexins, Cx43 is one of the most studied[43].

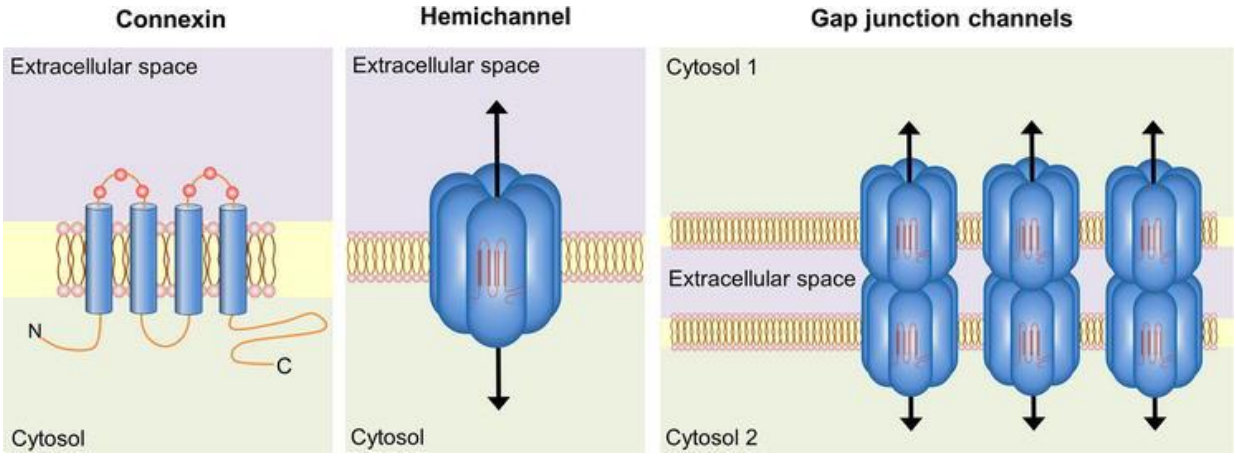

Figure 4: Overview of connexins, hemichannels and GJs[41].

1.8. Connexins in GB

Connexins are abundantly expressed in brain cells, including astrocytes[41]. Cx26, Cx30 and CX43 are expressed in the astrocytes in human, mouse and rat brain[41,44]. The main connexin expressed by astrocytes is Cx43[40,42]. Intercellular communication mediated via connexins plays a role in tissue homeostasis and regulation of cell growth and differentiation[43]. Tumour cells can interact with each other and with astrocytes via Cx43-based GJs to enhance their proliferation and invasive capacity[19].

Several studies describe the involvement of connexins in the development of GB. In GB, connexins are highly expressed, and the most frequent encountered connexin in GB cells is Cx43[45]. Crespin et al. used a tissue microarray technique and observed that more than 60% of GBs express Cx43[44]. Cx43 is found to be among the top 100 upregulated genes in patient tumour tissue as well as in primary glioma cell lines[46]. While Cx43 expression generally decreases with increasing glioma grade, it remains highly expressed in GB[45,46].

Sin et al. used two conditional knockout mouse lines in which Cx43 was eliminated in the astrocytes[47]. The absence of Cx43 in these astrocytes resulted in a reduction of the invasive capacity of the glioma cells into the brain parenchyma[47]. McCutheon et al. described that in higher-graded gliomas the expression of Cx43 is located towards the outer edge of the tumour[45]. This redistribution to the periphery implies that the core tumour cells are less well adhered to each other and this might be a consequence of the necrotic core[45].

Brain metastatic cells from lung and breast cancer form Cx43 GJs with astrocytes, which was shown by Chen et al.[48]. These metastatic cells transfer cyclic guanosine monophosphate–adenosine monophosphate (cGAMP), a secondary messenger, to astrocytes[48]. The transfer of cGAMP leads to astrocytic secretion of inflammatory cytokines, such as interferon alpha (IFNα) and tumour necrosis factor alpha (TNFα), which increase growth and chemoresistance

of cancer cells[49]. This was observed by co-culturing astrocytes with cancer cells. This co-culture revealed that IFN and nuclear factor kappa-light-chain-enhancer of activated B cells (NF-kB) pathways were activated in the brain metastatic cells, which suggests that signal transducer and activator of transcription 1 (STAT1) and NF-kB survival signals are triggered in cancer cells when GJs with astrocytes are formed[48].

Osswald et al. observed that Cx43-based GJs form communication routes in a multicellular network[46]. Moreover, they described that GB cells are able to form such a multicellular communication network, by forming so-called tumour microtubes (TMs), which contribute to the proliferation and invasion of GB[46]. GB cells situated more distant from the tumour core can also be connected via TMs, resulting in functional and treatment resistant cellular networks. Radiotherapy-induced cytotoxicity is caused by increases of intracellular calcium levels, and even small calcium increases can lead to intrinsic apoptotic cell death in glioma cells[46,50]. Intercellular TMs can serve as a means for individual tumour cells to distribute critical elevations of calcium within the larger network, achieving non-lethal levels[46,51]. This can explain how GB cells resist radiotherapy treatment[46].

These results show that Cx43 may have pro-tumorigenic properties. However, opposing roles are demonstrated for Cx43 in tumour invasion, growth and survival. For example, in 2007, Bates et al. observed that downregulation of Cx43 with the use of RNAi decreases the motility in C6 glioma cells, showing that Cx43 enhances glioma invasion[52]. In contrast to this finding, Aftab et al. reported that a reduction of Cx43 expression in the U118 human glioma cell line increased cell migration[53]. The same finding was observed when U87MG human glioma cells where co-cultured with astrocytes[54]. In addition, it was found that functional glioma-glioma GJs suppress glioma invasion, while glioma-astrocyte and astrocyte-astrocyte GJs promote invasion. The invasive effects of heterocellular GJs may arise from transfer of oncogenic signaling molecules from glioma cells to adjacent astrocytes via Cx43[55]. Furthermore, it is hypothesized that the role of Cx43 may be cell type-specific[56]. Gliomagenesis is characterized by different stages, during these stages different cell types are the drivers of tumour development. Thus, the role of Cx43 might differ from stage to stage[56].

Since connexins can facilitate malignant features, such as metastasis, growth and invasion, they may offer new therapeutic strategies in cancer. There are an increasing number of drugs available to inhibit GJ intercellular communication[43]. Yusubalieva et al. investigated a monoclonal antibody (MAbE2Cx43), targeting the second extracellular loop of Cx43. After intravenous administration of this antibody in rats with C6 glioma, glioma growth was reduced, and survival of the rats was increased[57]. Concomitant treatment with radiotherapy (total dose of 36 Gy) and this monoclonal antibody showed the same results[58]. MGMT-deficient GB patients develop resistance to TMZ, for this reason Murphy et al. used MGMT-deficient GB cells (SF-295, U87MG, and VTC-003) to induce chemotherapy sensitivity[59]. This resistance is mediated by Cx43 channel activity and the Cx43 C-terminus[60]. αCT1, a Cx43 C-terminus peptidomimetic increased the sensitivity to TMZ chemotherapy[59]. This peptide blocks Cx34 hemichannel activity and protein-protein interactions. Pridham et al. recently observed that Cx43 binds the p110β/p85 signaling complex, resulting in activated phosphatidylinositol-3-kinase (PI3K)/Akt signaling pathway, which renders GB cells resistant to TMZ[61]. αCT1 can block this interaction between Cx43 and p110β to overcome chemotherapy resistance[61].

1.9. Tonabersat

The therapeutic agent that will be used to target Cx43 GJs in this experiment is Tonabersat (SB-2022453). Tonabersat is a benzopyran derivate that binds to a unique stereoselective binding site in astrocytes and inhibits hemichannel or GJ-mediated processes[48]. This GJ inhibitor can pass the BBB, making it a potentially efficient treatment method[43]. Tonabersat inhibits Cx43 hemichannels at low concentration and Cx43 GJs at higher concentrations[62].

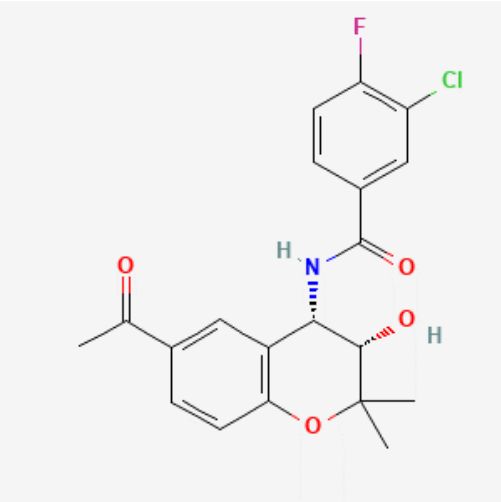

Figure 5: Chemical structure of Tonabersat (SB-2022453)

Source: National Center for Biotechnology Information (2022). PubChem Compound Summary for CID 6918324, Tonabersat. Retrieved December 1, 2022 from https://pubchem.ncbi.nlm.nih.gov/compound/Tonabersat.

1.9.1 Tonabersat in hemichannels

A lot of research has been done to find the molecular link between Cx43 hemichannels and inflammatory diseases[63]. A consequence of the opening of astroglial Cx43 hemichannels is the release of different transmitters, including adenosine triphosphate (ATP)[41]. An increase in ATP has been observed in CNS damage models in response to CNS injuries such as cerebral ischemia and spinal cord injury[63]. Cx43 hemichannel opening results in the activation of the inflammasome pathway by mediating an ATP autocrine feedback loop[62,64]. In addition, Cx43 hemichannels play a role in secondary lesion spread, edema, inflammation, gliosis and neuronal loss following CNS injury[62,63]. Kim et al. observed that Tonabersat directly inhibits Cx43 hemichannel opening in an *in vitro* and *in vivo* model of CNS injury[62]. In the *in vitro* ischemia-reperfusion model it was found that high concentrations of Tonabersat (> 100µM) resulted in uncoupling of GJs and internalisation and degradation of Cx43 via the lysosomal pathway. However, low concentrations of Tonabersat (10µM) blocked the ATP release of Cx43 hemichannels during injury and reperfusion, no effects on Cx43-based GJs were observed[62]. These findings were also observed in the *in vivo* rat bright-light injury model of retinal damage, which mimics age-related macular degeneration[62,63].

Lyon et al. showed that Tonabersat inhibited ATP-mediated inflammasome activation in an *in vitro* model using human retinal pigment epithelial cells[64]. This model mimics diabetic retinopathy (DR), which is a chronic retinal disease[64]. Inflammatory processes play a vital role in the pathogenesis of DR[63]. It was previously shown that DR is associated with the opening of Cx43 hemichannels, which activates the inflammasome, resulting in inflammation. Tonabersat has the potential to reduce this inflammasome-mediated inflammation in DR by blocking Cx43 hemichannel opening[64].

1.9.2 Tonabersat in cancer models

Brain metastatic cancer cells use Cx43-based GJs to transfer cGAMP to astrocytes, resulting in activation of the stimulator of interferon genes (STING) pathway and production of IFNα and TNFα[48]. These paracrine signals result in chemoresistance of the brain metastatic cells. Chen et al. demonstrated that Tonabersat inhibited the release of IFNα and TNFα in astrocyte cancer cell co-cultures, showing that Tonabersat breaks the paracrine loop[48]. Furthermore, they showed that treatment with Tonabersat inhibited brain metastasis from breast cancer in xenograft and immunocompetent mouse models[48]. Tonabersat (10 mg/kg) was administered daily, starting one day after cancer cell inoculation in mice. When used as a single agent a significant inhibition of the metastatic lesions was observed. Moreover, addition of the chemotherapeutic agent carboplatin to Tonabersat profoundly inhibited brain metastasis[48].

The therapeutic potential of Tonabersat for the treatment of GB in the F98 GB rat model has already been described by De Meulenaere et al.[25]. It was found that a combination of Tonabersat with radiotherapy (one dose of 20 Gy) and TMZ chemotherapy resulted in a

significant difference in tumour volume compared with the group receiving only the standard therapy (i.e. TMZ chemotherapy and radiotherapy). However, this study had some shortcomings[25]. The most significant one was the euthanasia of six rats due to the development of extended extra-cranial and/or extra-axial tumours. A possible explanation for the uncontrolled proliferation of the extra-cranial and extra-axial tumour is backflow of the F98 GB cells via the injection route after inoculation[25]. The early death of these animals ensured that no survival analysis was performed[25].

1.9.3. Tonabersat for the treatment of other disorders

Besides in the treatment of GB, the potential of Tonabersat has been examined in several other disorders. In 1999, Tonabersat was identified as a potential antimigraine agent in animal seizure models[65]. Its therapeutic efficacy has been tested in phase II clinical trials in patients for the prophylaxis of migraine. Tonabersat antagonises cortical spreading depression (CSD), which is characterized by a depolarisation wave that moves across the cortex, which is a known pathophysiological mechanism of migraine[65,66]. The events of CSD cause the aura phase that precedes migraine headache in about 20-30% of patients[67]. CSD leads to a cortical upregulation of genes involved in inflammatory processing, e.g. metalloproteinases[67]. Metalloproteinase activation results in leakage of the BBB, releasing molecules that sensitize the trigeminal nerve fibres[65,67]. In addition, CSD can activate dural nociceptors. In 2009 a randomised, double-blind, placebo-controlled crossover study to investigate the effect of Tonabersat on migraine with aura was performed[66]. Tonabersat (40mg/day) was compared with a placebo in patients who had at least one aura attack per month during the past three months. The result of this clinical trial showed that there was a significant reduction in the number of aura attacks when patients were treated with Tonabersat compared to the placebo[66]. There was no significant effect on the number of migraine headache days. No serious adverse events were reported during this trial, and Tonabersat was well tolerated by the patients[66].

Tonabersat has also been investigated as anti-epileptic drug. GJ communication is a potential mechanism for epileptogenesis and maintenance, because GJ-mediated electrical coupling can result in hypersynchronous neuronal activity, which is a characteristic of convulsive events[68]. Therefore, the occurrence of epilepsy can be controlled by GJ blockers, such as Tonabersat. Blower et al. observed that Tonabersat inhibited electrographic bursting in the K^+ hippocampal brain slice *in vitro* model in a dose-dependent manner[68,69]. Tonabersat attenuated tonic seizures induced with continuous intravenous (IV)-pentylenetetrazol in *in vivo* experiments in mice and rats[69]. In addition, Tonabersat significantly increased the threshold for electrically induced tonic extension seizures in both mice and rats. Based on these preclinical results, it has been proposed to test Tonabersat in phase I clinical trials for the treatment of epilepsy[70].

1.10. Magnetic Resonance Imaging

1.10.1. Basic physics

MRI is a medical imaging technique based on the interaction between an applied magnetic field and a nucleus[71]. This nucleus must have a nuclear magnetic moment, also called ‘spin’. The nuclei with an odd number of neutrons or protons exhibit spin[72]. For example, 1H, 31P, 13C, etc. have nuclear magnetic moments and are therefore suitable for detection by magnetic resonance[71]. Images can be made with each of these nuclei, but protons (1H) require the least time producing images with useful spatial resolution and optimal image quality[72]. This is partially due to the fact that protons are the most abundant nuclei in living organism and have the best MRI sensitivity[71,72].

These protons (H^+) carry a positive electrical charge and are constantly spinning[73]. This moving electrical field generates a magnetic field, leading to the fact that protons have an own magnetic field[73]. In normal conditions, the protons are randomly aligned, but when placed in

an external magnetic field (B_0) the protons will align parallel/antiparallel with B_0[71]. More protons align parallel with B_0 because this requires the least amount of energy[73,74]. This alignment yields a net nuclear magnetisation and a net magnetisation vector Mz parallel to B_0[71]. Nuclei wobble or precess around the direction of magnetic field B_0[74]. The frequency of this precession is called the Larmor frequency (ω). The formula of the Larmor frequency is $\omega_0 = \gamma B_0$, γ is the gyromagnetic ratio[73]. The Larmor frequency is proportional to the magnitude of B_0[71].

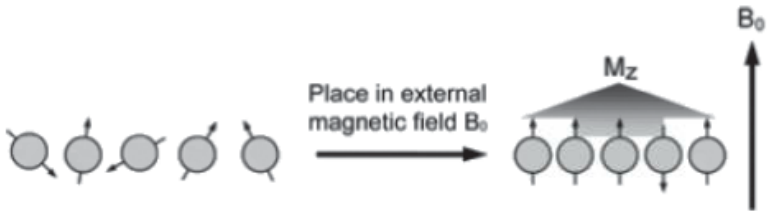

Figure 6: Randomly aligned protons will align parallel or anti-parallel with the external magnetic field B_0. This results in the magnetization vector Mz[71].

The vector Mz can be flipped from the longitudinal z-axis towards the transverse xy-plane by applying a time-dependent radiofrequency (RF) pulse at the Larmor frequency perpendicular to B_0[71]. This process is called transverse magnetisation. The applied RF pulse forces the protons to move in phase, meaning that they will all precess at the same time[73]. This rotating transverse magnetization will induce an alternating current in the receiver coil and can be measured, resulting in an MRI signal[73,74].

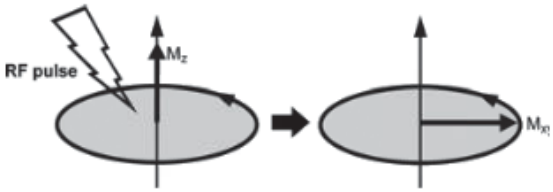

Figure 7: Application of an RF pulse can flip the magnetization vector Mz to the xy-plane[71].

To form the final MR image, it is necessary to determine the location of the signal[72,74]. Slice selection gradient, frequency encoding gradient and phase encoding gradient are the three magnetic field gradients used for this localisation[73,74]. The slice selection occurs through a gradient field generated by gradient coils. This gradient field alters the strength of B_0 in the chosen direction, resulting in protons with different Larmor frequencies within the gradient field[73]. The RF pulse, which is applied to move the magnetization vector out of alignment with B_0, consists typically of a small range of frequencies[73]. This excites a slice of certain thickness. To obtain information of the individual points (pixels) within a slice, frequency and phase encoding gradients are used[73,74]. After application of the RF pulse, the protons all precess in phase in the xy-plane[73]. By applying a new gradient magnetic field some of the protons will precess faster than the other protons, depending on their position in the gradient. The shift of phase in precessing depends on the duration of this gradient switch[74]. Switching this gradient off results in protons with the same precession frequency but they will no longer be in phase[73]. This allows the protons to be differentiated and is called phase encoding. Lastly, the frequency encoding gradient is used to differentiate the pixels with the same phase encoding[74]. This gradient is applied perpendicular to the phase encoding gradient, causing the protons to rotate at different frequencies[73].

This sequence of slice selection, phase encoding and frequency encoding is repeated many times because the RF pulse excites all protons in a slice and one single echo signal is recorded for one phase encoding step[73]. For each repetition the same slice selection and frequency encoding gradient is used, but the strength of the phase-encoding gradient is increased. For each step, a signal echo is digitised and stored in a raw data matrix, this is called the 'k-space'[73]. Each data point in the k-space has Kx and Ky coordinates, these define the spatial frequency in the X and Y directions[72]. Horizontal stripe patterns are represented by points along the Ky axis and vertical stripe patterns by points along the Kx axis. The array of spatial

frequencies used to form the final image is in this way summarized in the k-space[72]. With the use of a Fourier transform of the k-space the final MR image is created[72,73].

When the RF pulse, that induced a switch from the Mz vector towards the xy-plane, is switched off, the protons will go back to the lower energy equilibrium phase[74]. This means that the induced signal in the receiver coil will decrease in time, this decrease is called the free induction array (FID). The term relaxation time refers to the time required for the signal to return to the equilibrium[74]. This relaxation process occurs in two different ways. The transverse magnetisation in the xy plane starts to disappear, this is known as transverse (or T2) relaxation[71,73]. T2 shows the loss of phase coherence of the protons and is the time taken by the magnetisation to decay to 37% of its initial value[71,74]. Secondly, the longitudinal magnetisation in the z-plane starts to return, this is called longitudinal (or T1) relaxation[73]. T1 relaxation time is the time taken by the spins to reach up to 63% of the equilibrium value[71,74]. Time-independent inhomogeneities in B_0 can induce an additional dephasing, resulting in a decay shorter than T2, called T2*[71]. The different relaxation times ensure that there is contrast present in the final MR image. Images that show T1 relaxation time, are called T1-weighted (T1w) images, likewise images showing T2 relaxation time, are called T2-weighted (T2w) images. T1w images are generated by manipulating the time between two RF pulses, this is called the repetition time (TR)[73]. The time between the selective excitation pulse and the peak of the MRI signal is the echo time (TE) and is used to determine the amount of T2 weighting in an image[72].In addition, proton density, which is a representation of the number of protons in a volume of tissue, contributes to the development of contrast[71]. Various human tissues have different T1 and T2 values, but T2 relaxation time is always shorter than the T1 time[74]. Tissues with a short T1 are displayed bright on T1w images, in contrast to tissues with long T1 time, which appear dark in T1w images because they relax slower and emit fewer signals[71]. For T2w images this is reversed, tissues with short T2 appear dark, while tissues with long T2 appear bright[71].

1.10.2. Components of an MRI system

An MRI system consists of four main components: a main magnet, gradient coils, RF coils and computer systems[75]. The magnetic field B_0 is generated by the main magnet and is measured in units of Tesla (T)[75,76]. Currently, most clinical MR systems are superconducting and operate at 1,5T or 3T[73]. Few 4T magnets are used for clinical studies[77]. 7T, 9.4T, 10.5 and 11.7T MR systems have already been developed. The last years researchers have been looking to achieve magnets at fields of 14T and even 20T[77]. Currently, the first 14T MRI is being produced in the Netherlands. MRI at these high fields can provide researchers with significant information about human biology[77].

The superconducting magnet is composed of a series of coils, the magnetic field is generated when a current is passed to the coils by an external power source[75]. The coils become superconducting at temperatures below 10 Kelvin (-263°C)[73,75]. At this temperature, the resistance to the flow of the electric current is reduced[73]. The lower the resistance, the higher electric currents can be used to produce high-strength magnetic fields. This temperature is achieved by cooling the coils in a bath of cryogenic liquid helium enclosed in a cryostat[73,75].

In addition to the main magnetic coils, there are three gradient coils, representing the three orthogonal directions[73]. These can generate a magnetic field in the same direction as B0 but with a strength that changes along the x, y or z axis[73,75]. Gradients allow spatial encoding of the MR signal[75].

RF coils generate an electromagnetic field, referred to as B_1, that lies in the megahertz (MHz) range[73]. These coils are the most important determinants of signal-to-noise ratio (SNR) and signal uniformity[75]. RF coils can be transmitter coils, receiver coils or combined transmitter-receiver coils. These transmitter coils transmit RF energy and the receiver coils receive the induced RF signal from the tissue[73]. RF coils can also be divided into volume coils and surface coils[75]. Volume coils cover large fields of view, while surface coils are placed on the limited

anatomy of interest and therefore have small fields of interest[75]. For neuroimaging, a separate surface RF coil is placed around the head to detect the emitted MR signals and therefore improve SNR[73]. Lastly, there are also shim coils. These are used to adjust the magnetic field and improve its homogeneity[73].

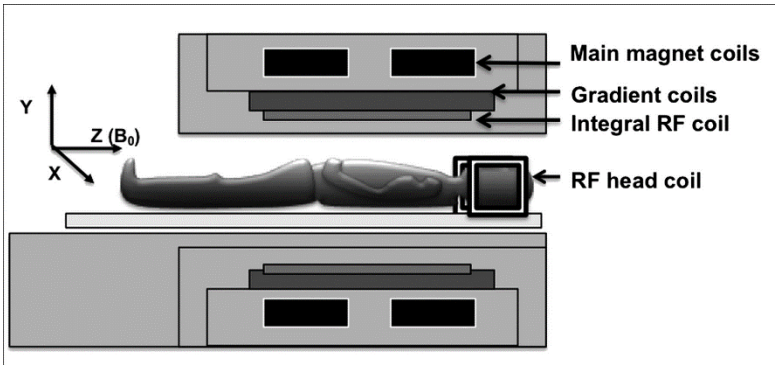

Figure 8: Schematic illustration of the different coils in an MR machine. Main magnetic coils, gradient coils and RF coils are shown. In addition to these coils, there are also shim coils. For neuroimaging, an additional RF coil can be placed around the head of the subject[73].

1.10.3. Contrast agents

The extent to which a substance becomes magnetised when placed in an external magnetic field, is known as magnetic susceptibility[73]. Biological tissues are negligible susceptible, while matter such as iron are extremely susceptible. To increase the difference between normal and abnormal tissue on an MRI image, contrast agents can be used[78]. These contrast agents can be administered intravenously, orally or by inhalation[79].

Intravenously administered contrast agents can be categorized in three types: extracellular fluid (ECF), blood pool and target/organs specific agents[79]. ECF agents travel to the heart after injection, from there they go to the systemic arteries and leak into the extravascular, extracellular space. Blood pool agents stay in the intravascular space after injection. The organ-specific agents are capable of targeting specific organs or tissues[79].

The contrast agents that are mostly used for MRI are either superparamagnetic magnetite particles or paramagnetic Gd ion complexes[78]. The superparamagnetic iron oxide contrast agents can be divided into two types, namely; superparamagnetic iron oxide (SPIO) and ultrasmall superparamagnetic iron oxide (USPIO)[78]. Because SPIO nanoparticles accumulate in the liver, it is considered a liver-specific T2 contrast agent[80]. Recently, USPIO nanoparticles are receiving more attention because of the outstanding T1-weighted MRI performance, biocompatibility, long blood circulation and reduced organ accumulation. These advantages make USPIO nanoparticles potent candidates for a wide range of MRI applications, such as tumour, atherosclerosis and inflammation imaging[80].

The paramagnetic contrast agents are usually made from the lanthanide metal Gd (Gd^{3+}) or the transition metal manganese (Mn^{2+}). Gd possesses a high magnetic moment and is the most stable ion with unpaired electrons[78]. These unpaired electrons can interact with adjacent protons, in this way these protons will relax more rapidly. Because of this feature, it is the most used metal atom in MRI contrast agents. For about 60% of neuro MRI exams Gd-based contrast agents are used[79]. Dotarem, Gadovist, Magnevist, etc. are examples of Gd-based contrast agents that are used in the clinic[78,79].

These Gd-based contrast agents shorten the T1 and T2 relaxation time, resulting in an increase of the signal intensity of T1w images and a decrease of the signal intensity of T2w images[78]. The signal increased in T1w images is better visible than any corresponding signal decrease in T2w images[73]. The shortening of T1 relaxation time happens when low Gd concentrations are used[78]. Therefore, T1 images are evaluated in clinical practice because high Gd concentrations lead to an increased risk of toxicity[78]. Currently, Gd is coupled to the chelating agent diethylenetriamine pentaacetic acid (DTPA) to reduce the high toxicity of unchelated Gd[81].

Gd-based contrast agents have a molecular weight of 550 to 600 Da, which prevents them from crossing the BBB[82]. When there is BBB leakage or dysfunction in case of pathological disruption, these contrast agents are free to leave the vascular space. Tumours gain greater concentrations of contrast agents because they are hyper-vascularised and have a compromised endothelium[79]. Thus, minutes after the intravenous injection of the contrast agent, contrast enhancement of the tumour is observed[79].

1.10.4. MRI in GB

MRI allows detailed structural evaluation of the brain and intracranial neoplasms[83]. Therefore, MRI is the imaging technique used for diagnosis, characterization, surveillance and therapeutic monitoring of GB[84]. For the diagnosis of intracranial malignancies typically T1w, T2w, fluid attenuated inversion recovery (FLAIR), T2*w gradient echo and contrast enhanced T1w images are used[83,84]. Gliomas appear hypointense on T1w images and hyperintense on T2w images[83]. A common characteristic of GB is the presence of contrast enhancement with central necrosis in which there is an irregular ring enhancing lesion with central T2 hyperintensity. There is currently an increasing interest to find a correlation between MRI tumour characteristics with relevant molecular and genetic features[83].

High resolution MRI can be used for surgical planning and intraoperative guidance[84]. This imaging technique can identify tumour progression and important characteristics including the volume of the tumour and tumour sub-regions (necrotic, enhancing and non-enhancing), compression of the surrounding tissue and midline deviation. Nowadays, advanced MR techniques such as perfusion-weighted imaging, MR spectroscopy and diffusion-weighted imaging can be used to yield important information on tumour infiltration, aggressiveness and treatment response[83].

1.11. Models for GB

In vitro and *in vivo* models for human GB are used to understand more of the tumour biology[85]. Moreover, they facilitate the development of novel therapeutic strategies and study of the effectiveness of existing treatments for tumours[85,86].

1.11.1. Characteristics of a GB model

A good preclinical GB model needs to resemble the characteristics of human GB well; therefore, it is important that the model meets certain criteria. The model needs an adequate microenvironment with regard to immunocompetence, presence of BBB and cell-cell interaction[85]. In addition, the intratumoural cell heterogeneity requires to be similar to human glioma. Other histological features that need to be present in the GB model include necrosis, microvascular perfusion and rapid infiltrating growth[87].

1.11.2. Animal models

In vivo animal studies are necessary to explore the fundamental biology or test therapeutics in a way that is not possible by working directly with human patients[88].

1.11.2.1. Murine models

The most frequently used chemically induced mouse glioma model is the GL261 glioma[89]. The first time this cell line was generated by intracranial (i.c.) injections of methylcholanthrene (MCA), followed by serial i.c. and subcutaneous transplantation of tumour fragments in C57BL/6 mice[85,89]. Nowadays, 1 x 10^5 GL261 tumour cells are inoculated in these mice to generate this model[90]. GL261 is a syngeneic, meaning that these mice have the same genetic background as the mice in which the cell line was produced, mouse model in C57BL/6 mice[90]. These mice do not require a deficient immune system, which results in a model that mimics the growth and immune response of human GB[87,90].

Another murine glioma model is the U87. This is a xenograft model induced by the implantation of patient-derived glioma cells into immunodeficient mice[89]. This model can be generated by intracranial injection of concentrations of 1 x 10^5–1 x 10^6 of U87 cells suspended in 5–10 ml,

and injections at approx. 1 mm anterior and 3 mm lateral to the bregma inserted 3–4 mm deep into the or right striatum of athymic nude mice[90]. These athymic nude mice lack hair, but more important is the absence of a thymus, resulting in a deficiency of T-lymphocytes, which immunocompromises the mice[91]. This deficiency of T-lymphocytes allows the engraftment, growth and metastasizing of tumour cells. U251 malignant xenograft glioma model is generated the same way[85]. This model is known to mimic the features of human GB[90]. A disadvantage of the use of immune-deficient mice is that there will be a selection for the fastest growing cells resulting in a reduced intratumour heterogeneity[85].

The molecular biology and the knowledge of the driver mutations that are involved in gliomagenesis has been evolving and nowadays genetically engineered mouse models (GEMMs) are often used[85,88]. GEMMs can be generated via multiple methods, for example, via a transcranial injection of a lentivirus, which expresses the cre-recombinase under control of the glial cell-specific GFAP promotor. This injections takes place in a LoxP-transgenic mice, conditionally lacking p53 or pten and overexpressing the constitutively active $KRAS^{v12}$ [85]. Cre-Lox is a recombinase, which produces recombination between 2 pairs of loxP sites, which leads to insertions or deletions in the mouse genome[89]. After administration of Cre in these mice, high-grade gliomas develop[85]. GEMMS are suitable to investigate genetically defined gliomas, but they lack the intratumour heterogeneity that is found in human GB[85].

1.11.2.2. Rat models

The three most commonly chemically induced used rat brain tumour models are the C6, 9L and F98 gliomas[89,90]. The C6 glioma cell line was developed by repetitive intravenous administration of methylnitrosourea (MNU) in adult (>8 months) Wistar-Furth rats[89,90]. This model can now be generated by implanting 1 X 10^5 cells in a 5µl suspension into the fronto-parietal lobe[90]. The C6 glioma cells do not require to be implanted in syngeneic Wistar-Furth rats, Sprague-Dawley and Long-Evans rats also allow engrafting of C6 cells without rejection[90]. The C6 glioma model does not display necrosis, nuclear polymorphism and high mitotic rates as can be found in human GB. Another disadvantage is the fact that the C6 glioma is immunogenic, Wistar rats implanted with C6 glioma cells developed potent humoral and cellular immune responses to the tumour[89].

The 9L gliosarcoma cell line was also generated by a repetitive administration of MNU in Fischer 344 rats[90]. 1 x 10^5 tumour cells in a 5µl cell suspension is usually injected into the striatum to generate this model. After implantation in syngeneic Fischer rats, rapidly growing tumours that are composed of spindle-shaped cells with a sarcomatous appearance develop[89]. The 9L gliosarcoma is highly immunogenic, this has to be kept in mind when using this model to evaluate the efficacy of novel therapeutic strategies[89,90].

The F98 cell line was produced by intravenous administration of a single dose of ethylnitrosourea (ENU) (50mg/kg bodyweight) to a pregnant Fischer 344 rat on the 20th day of gestation[89]. The embryos are in utero exposed to this DNA-damaging agent, inducing brain tumours in the offspring[85]. These tumours were propagated *in vitro* and cloned[92]. ENU-induced gliomagenesis gives rise to genetically heterogeneous tumours and involves a proper tumour microenvironment, including an intact immune system and BBB[85]. The F98 GB rat model is less immunogenic than the C6 and 9L rat models and is therefore in particular very useful for the evaluation of therapeutic agents[89].

Another rat glioma model that is less frequently used is the non-immunogenic CNS-1 glioma model[90]. This cell line was generated by intravenous administration of MNU to young rats for 36 weeks. 1 x 10^5 tumour cells are usually injected into the striatum to develop this glioma rat model[90].

1.11.2.3. Advantages and disadvantages of rat versus murine models

Rat models have many advantages over the mouse models[89]. Most of the advantages of rat models have to do with the size of the brain. The larger size of the rat brain helps inoculating the cells more precisely and allows a larger tumour size, which results in a better *in vivo*

localisation by various imaging methods[89]. In addition, the larger brain makes it easier to produce images with better spatial resolution[87,89]. Rat models have a longer interval of time before death because the bigger size of the brain allows a bigger tumour to grow[87,89]. Larger amounts of therapeutic agents can be administered intracerebrally in rat models. Lastly, there is more literature on rat brain tumours compared to mouse brain tumours[89].

But there are also disadvantages of the use of rat models. Rats are more expensive to purchase and maintain and few genetically engineered tumour cell lines are available[89,92]. In addition, it is easier to achieve genetic manipulation in mice (e.g. GEMMs), allowing the study of genetic factors and signaling pathways[87,89].

1.11.2.4. Alternative animal models

The *Caenorhabditis elegans* and *Drosophila melanogaster* are cost-effective alternatives to mammalian studies[88]. *Danio rerio* is another vertebrate animal model that can be used for imaging studies and the visualisation of the tumour cells *in vivo*, because of the transparency of this zebrafish[88]. However, the use of non-mammalian species has some limitations. The complex segmented CNS, which is present in humans, is lacking in these species[93]. In addition, there is homology with the genes of humans but there is also redundancy due to the genetic duplication within the genome of non-mammalian species. This complicates the use of transgenic models. Lastly, these species are smaller than mammalian species which might pose technical challenges to perform experimental studies[93].

Large-animal models of GB offer significant anatomical, physiological and genetic advantages[86]. Recently porcine glioma models, but also canine models have been generated. The brain of the pig is gyrencephalic, resembling more the human brain compared to rodents. In addition, the size of pigs offers significant benefits for high-resolution imaging of the brain[86]. Dogs can spontaneously develop GB, which offers the opportunity to study GB in absence of inductive factors[86]. These spontaneously arising canine gliomas are analogue to the human gliomas[94]. Lastly, non-human primates can be used, they are phylogenetically closer to humans and resemble the human brain anatomy. However, ethical considerations have limited their use as preclinical models[86]. In 2017, a tree shew GB model was generated by an intracranial injection of a lentivirus that overexpressed the constitutively active Harvey Rat Sarcoma Viral Oncogene Homolog (H-RAS) and silenced the Tp53 gene[95]. The tree shrew is a small primate-like animal and is evolutionary closest to the primate. This GB model showed more similarities to the human GB than mouse models generated the same way[95].

1.11.3. MRI in animal models

In the past, changes in tumour growth and tumour physiology were observed via invasive methods and animals had to be killed at predefined time-points to perform longitudinal studies[96]. Nowadays, MRI is used as a non-invasive *in vivo* imaging method to follow the dynamic disease process in animal models[97]. The use of MRI is in compliance with the 3R (Reduction, Refinement, Replacement) principle in animal research[98,99]. Each animal serves as its own control, resulting in an alleviation in biological variability and smaller group sizes. This imaging technique causes as little distress as possible, which complies with refinement[99]. In addition, the animals are not exposed to harmful ionizing radiation by the use of MRI[97].

Most of the small animal MRI systems operate at 4.7T – 11.7T field strength[97]. But with higher field strength, more artefacts and other limitations occur. Therefore, the 7T magnet is the most commonly used among animal research facilities[97]. This is a high field strength, in comparison to the standard clinical range of 1,5-3T used for human subjects. The main advantage of this high field strength is the increased SNR, which results in a higher resolution acquisition[97,99].

Physiological noise generated by the amount of movement an animal induces through breathing is an important problem in animal imaging[99]. Therefore the animal must be anesthetised, which is usually achieved by the inhalation of isoflurane[97,99]. Inhalational anaesthesia is administered continuously and can be adjusted to the requirements of the animal[97]. Isoflurane is well tolerated and animals breathe spontaneously and do not require

endotracheal intubation[99]. Another important factor that can help with this immobilisation is a probe, which keeps the animal stable during the imaging session[97]. Many animal research institutes develop custom-made holders for maximal stability[97].

1.12. Research aim

In this study, we investigate whether targeting Cx43-mediated communication by using a pharmacological inhibitor, such as Tonabersat, might provide new and potent ways to improve the standard medical treatment of GB. A new treatment strategy is urgently needed for GB patients since the current therapy fails to improve the overall survival. The efficacy of the current radiotherapy and TMZ chemotherapy treatment is limited due to therapy resistance and tumour recurrence.

The aim of this experiment is to investigate the most potent combination of fractionated radiotherapy, TMZ chemotherapy and/or Tonabersat for the treatment of GB. The standard therapy, consisting of radiotherapy and TMZ chemotherapy, will be compared with the standard therapy combined with Tonabersat. For this comparison statistical analysis of the brain tumour volumes and a survival analysis will be performed. In addition, we investigate the interaction of Tonabersat with radiotherapy or TMZ chemotherapy to observe if Tonabersat is radiosensitive or chemosensitive. Therefore, the hypothesis of this study states that Tonabersat combined with one of the other treatment possibilities will lead to a significantly reduced volume of the tumour in the brain and possibly a prolonged survival time. De Meulenaere et al. demonstrated that Tonabersat has an adjuvant therapeutic potential when used in combination with radiotherapy and TMZ chemotherapy[25]. This was observed in terms of tumour volumes, which remained more stable over time. However, we will make use of fractionated radiotherapy (3 doses of 9Gy), which leans more towards the standard of care.

To test our hypothesis, the recently optimized F98 GB rat model will be used. Four treatment groups will be investigated. The first treatment group receives fractionated radiotherapy and TMZ chemotherapy, this group is called the standard therapy group and serves as a control group. The standard therapy + Tonabersat group receives the same treatment as the control group, but these rats receive additional daily injections of Tonabersat. Thirdly, there will be the TMZ chemotherapy + Tonabersat group, receiving only injections of TMZ chemotherapy and Tonabersat. Lastly, the rats from the fractionated radiotherapy + Tonabersat group receive fractionated radiotherapy and daily injections of Tonabersat.

2. Materials & methods

The following methods were previously described by De Meulenaere et al.[25] and Bouckaert et al.[100].

2.1. Cell culture of F98 GB cells

F98 GB cells were cultured using Dulbecco's Modified Eagle Medium (DMEM) supplemented with 10% Fetal Bovine Serum (FBS), 1% Penicillin-Streptomycin antibiotics, 0,1% fungizone (amphocyterine B) and 1% pyruvate. The cells were kept in an incubator at 37°C and 5% CO_2.

2.2. Approval ethics committee

This study protocol was approved by the animal ethics committee of the Faculty of Medicine and Health Sciences of Ghent University (ECD 21/06).

2.3. Housing conditions

All animals were kept and handled according to European guidelines (Directive 2010/63/EU) and housed under environmentally controlled conditions: 12 h light/dark cycle, temperature: 21-24 °C, and relative humidity: 40% - 70%, daily monitoring of these conditions was performed. Food and water were provided *ad libitum*.

2.4. Experimental setup of F98 GB model

2.4.1. Inoculation

Inoculation of F98 GB cells into the right entorhinal cortex of ten-weeks old female Fisher rats was performed to develop the F98 GB rat model. The rats were anaesthetised with isoflurane mixed with oxygen administered at a flow rate of 0,5 l/min (induction: 5% and maintenance: 2%-3%, depending on several factors including health status and bodyweight of the rat). Subsequently, the rat was immobilized in a stereotactic frame using ear bars and shaved from eye to ear. Next, xylocaine and adrenaline (0,1 ml) were injected in the head region, followed by swabbing the head with chlorhexidine (Iso-Betadine®). The skull was exposed through a longitudinal incision. Afterwards, a 1 mm hole (anterioposterial (AP): −8.0 mm and mediolateral (ML): +4.5 mm relative to bregma, dorsoventral (DV): −4.1mm relative to dura) was made using a diamond drill (Dremel®) in the right entorhinal cortex. A 5 µl cell suspension of 5000 F98 GB cells was injected with the use of a stereotactically guided insulin syringe. Five minutes post inoculation the syringe was slowly withdrawn in steps of 0,7 mm, each step lasting two minutes. Afterwards, the incision was closed with resin-based dental cement (Simplex Rapid fluid/powder, Kemdent, UK), Metacam® (1ml/kg) was injected subcutaneously in the neck region and the skin was sutured. Lastly, a small smear of Neobacitracine was applied on the surgical wound.

2.4.2. MRI confirmation of GB growth

Seven days post-inoculation, a contrast-enhanced T1-weighted (CE T1w) sequence (SE RARE, 117 µm in-plane resolution, TR/TE 1539/9.7 ms, 3 averages, TA 4'15") was performed using a 7-Tesla system (Pharmascan 70/16, Bruker, Ettlingen, Germany) to confirm GB growth. The rats were anaesthetised with isoflurane (induction: 5%, maintenance: 2%), mixed with oxygen. Subsequently, Gd-based contrast (1mmol/kg Gadovist, Bayer, Leverkusen, Germany) was intravenously administered in a tail vein with the use of a 30-gauge needle. Afterwards, the rat brain surface coil (Rapid Biomedical, Rimpar®, Germany) was placed around the head and a heart monitor was placed underneath the animal. Then, the bed was shoved into a 72 mm rat whole body transmitter coil (Rapid Biomedical, Rimpar®, Germany) and a CE T1w image was acquired. For visualisation of this image the Pharmascan® 360 (Bruker, Ettlingen, Germany) software was used.

The GB tumour growth is confirmed by CE T1w MRI when the diameter of the tumour is approximately 2-3 mm, thereafter the rats were randomly assigned into a standard medical treatment group (n=7), a standard medical treatment and Tonabersat group (n = 7), a

fractionated RT and Tonabersat group (n=7), and a TMZ chemotherapy and Tonabersat group (n=6).

2.4.3. Treatment protocol

2.4.3.1. Fractionated radiotherapy treatment

First, Gd-based contrast (1 mmol/kg, Gadovist, Bayer, Leverkusen, Germany) was intravenously administered in a tail vein. Next, the rat was placed on a multimodality bed and a CE T1w MRI scan was performed for tumour localization. The rat is transported on the multimodality bed to the four-axis robotic positioning stage of the SARRP (Small Animal Radiation Research Platform). First, a planning CT (720 projections acquired over 360°) was performed. The data of the CT scan was then uploaded in the treatment planning software (Muriplan). Co-registration with MRI was performed manually. Based on this co-registered image, the isocenter was set in the middle of the tumour region. 3 fractions of 9 Gy were delivered by applying a single static beam parallel to the inoculation tract, and two non-coplanar arcs (120°) using a 5 x 5 mm collimator (voltage X-ray source: 220 kV).

2.4.3.2. Temozolomide chemotherapy treatment

TMZ (MedChem Express, New Jersey, United States) was first dissolved in 20% DMSO and diluted to maximal 1 ml with phosphate-buffered saline. First, the rats were anaesthetised (isoflurane mixed with oxygen; induction: 5%, maintenance: 2%). Subsequently, intraperitoneal injections of 29 mg/kg TMZ were administered for 5 consecutive days starting at the day of RT (i.e. day 1).

2.4.3.3. Tonabersat treatment

Tonabersat (MedChem Express, New Jersey, United States) was first dissolved in 10% DMSO, 10% Tween20 and diluted to maximal 1 ml with phosphate-buffered saline. First, the rats were anaesthetised (isoflurane mixed with oxygen; induction: 5%, maintenance: 2%). Subsequently, intraperitoneal injections of 10 mg/kg Tonabersat were administered daily, starting at the day of GB growth confirmation (i.e. day 0) until humane endpoints were reached.

2.4.4. Treatment groups

2.4.4.1. Standard Medical Treatment Group (control group)

Starting the day after GB tumour growth confirmation (i.e. day 0), the rats received TMZ chemotherapy (29 mg/kg, 5 consecutive days: day 1-5) and fractionated RT (3 fractions of 9 Gy on day 1, 3 and 5).

2.4.4.2. Standard Medical Treatment and Tonabersat Group

Starting the day after GB tumour growth confirmation (i.e. day 0), the rats received TMZ chemotherapy (29 mg/kg, 5 consecutive days: day 1-5) and fractionated RT (3 doses of 9 Gy on day 1, 3 and 5). In addition, Tonabersat (10 mg/kg) was administered daily from the day of GB tumour growth confirmation until the humane endpoints were reached.

2.4.4.3. Fractionated RT and Tonabersat Group

Starting the day after GB tumour growth confirmation (i.e. day 0), the rats received fractionated RT (3 doses of 9 Gy on day 1,3 and 5). In addition, Tonabersat (10 mg/kg) was administered daily from the day of GB tumour growth confirmation until the humane endpoints were reached.

2.4.4.4. TMZ chemotherapy and Tonabersat Group

Starting the day after tumour growth confirmation (i.e. day 0), the rats received TMZ chemotherapy (29 mg/kg, 5 consecutive days: day 1-5). In addition, Tonabersat (10 mg/kg) was administered daily from the day of GB tumour growth confirmation until the humane endpoints were reached.

2.4.5. MRI follow-up for the evaluation of tumour growth

To follow-up GB growth, CE T1w MRI sequences were performed on day 6, 9, 12 and every following three days. The start of treatment was considered as day 1 and scans are performed until humane endpoints were reached.

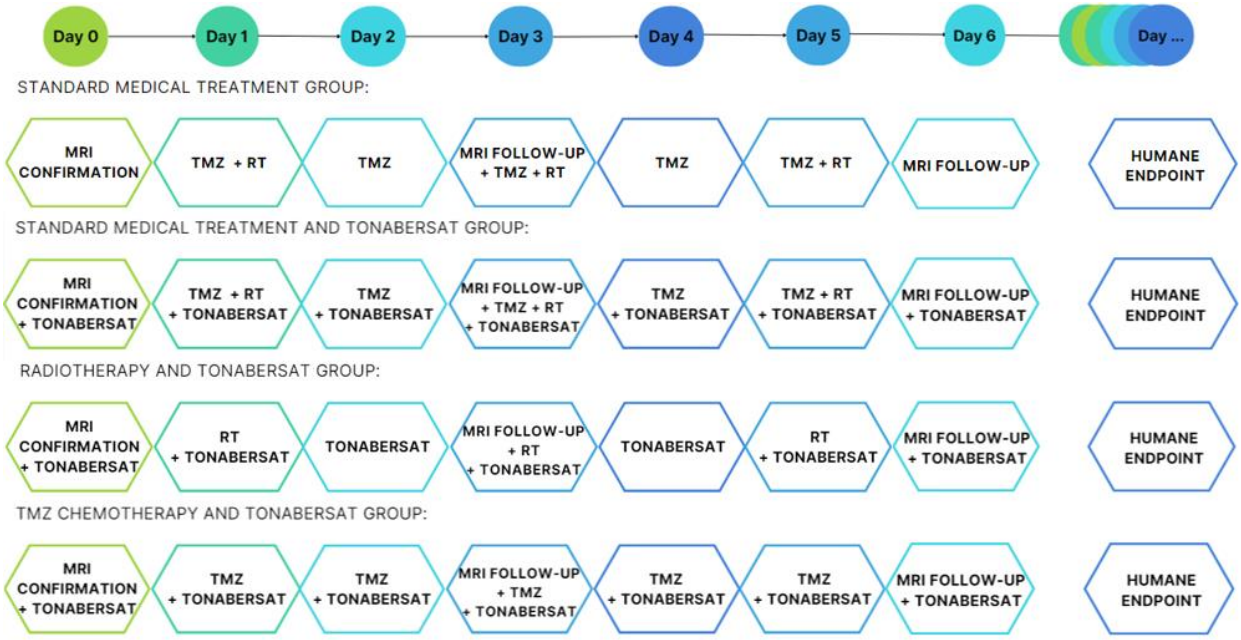

Figure 9: Overview of the different treatment groups and the treatments they receive starting at the day of confirmation (i.e. day 0). Abbreviations: Temozolomide (TMZ), fractionated radiotherapy (RT).

2.4.6. Euthanasia

The rats were daily weighted and monitored for the development of symptoms of discomfort and pain. According to the humane endpoints, rats were euthanized using an intravenous injection of pentobarbital (100 mg/kg, Kela, Hoogstraten, Belgium), when signs of behavioural changes such as reduced activity, absence of grooming and balance problems were observed. In addition, weight loss of 20% of the initial bodyweight and a tumour volume (monitored by MRI) of 40% of the total brain volume were indications to immediately euthanize the animals.

2.5. Histological analysis

For each treatment group, the brain of one at random chosen rat was isolated, washed with PBS and immersed for 24-48 hours in 4% paraformaldehyde and embedded in paraffin. For the histological confirmation of the presence of GB, the cerebrum was sectioned in 5µm slices and stained with Haematoxylin and Eosin (H&E). An immunohistochemical staining for Cx43 was performed to determine Cx43 expression. To evaluate reactive astrocytes, immunohistochemical staining for Glial Fibrillary Acidic Protein (GFAP) was performed. Both immunostainings required an incubation with serum whereafter an incubation with primary antibodies (i.e. Cx43 and GFAP) took place. Subsequently, an incubation with biotinylated secondary antibodies and streptavidin-peroxidase complex and 3,3' diaminobenzidine peroxidase solution was performed. Finally, the sections were counterstained with haematoxylin (Mayer) and coverslipped using mounting medium (4111, Richard-Allan Scientific, Thermo Fisher Scientific).

2.6. Statistics

2.6.1. Survival analysis

A survival analysis was performed using the Kaplan-Meijer method. The log-rank test was used, followed by a Holm post-hoc analysis. Differences with a P-value below 0,05 were considered statistically significant.

2.6.2. Statistical analysis

The software Fiji (Fiji Is Just ImageJ, version v1.52p) was used to measure the tumour areas on the CE T1w MRI images. By multiplying these areas by the slice thickness (0,6mm) the GB volume (mm^3) was determined per measured time-point. An overview of the GB volumes (mm^3) per animal per time-point can be found in the table A1 (*Addendum*). The statistical analysis was performed using RStudio (version 2023.03.0-386). The data was log-transformed to comply with the normality assumption needed for the statistical tests used during the analysis. A QQ plot, homoscedasticity plot and residual plot were generated to confirm, respectively, the normality, homogeneity of variances in different groups and linearity of the log-transformed data (see *Addendum*: fig.A1-A3).

A one-way ANOVA test of the log-transformed data was computed to make sure that there were no significant differences between the mean tumour volumes of each treatment group on the day of GB confirmation (i.e. day 0). To test the differences in tumour volumes of all the treatment groups on multiple time-points, a linear mixed model, with correction for multiple comparisons using the Bonferroni method was used. There are two reasons for choosing this statistical test for the analysis. First, during the experiment multiple tumour volumes were measured in one rat at different time-points. Secondly, the rats were euthanized at different time-points, which leads to missing data according to the missing-at-random principle. Differences with a P-value below 0,05 were considered statistically significant.

3. Results

3.1. GB volume and mean rates of tumour growth

3.1.1. Comparison tumour volumes on day 0

The mean duration between inoculation and GB confirmation (i.e. day 0) for all animals is 10 days (standard deviation ≈ 1,6) (*Addendum* figure A4). Two outliers (32 days and 41 days from inoculation until GB confirmation) in the RT and Tonabersat group were not included to calculate this mean and standard deviation.

In figure 10 the GB volumes (mm³) on the day of GB confirmation (i.e. day 0) for all animals in the four treatment groups (i.e. standard therapy (ST), standard therapy + Tonabersat (ST + T), TMZ chemotherapy + Tonabersat (TMZ + T) and radiotherapy + Tonabersat (RT + T)) are shown in a boxplot. The mean GB volume (mm³) on day of GB confirmation and the standard deviation for each treatment group is added to this figure. The one-way ANOVA statistical test of the log-transformed data showed that the differences between the mean tumour volumes on day 0 between the four different treatment groups are not significantly different (p-value = 0,83).

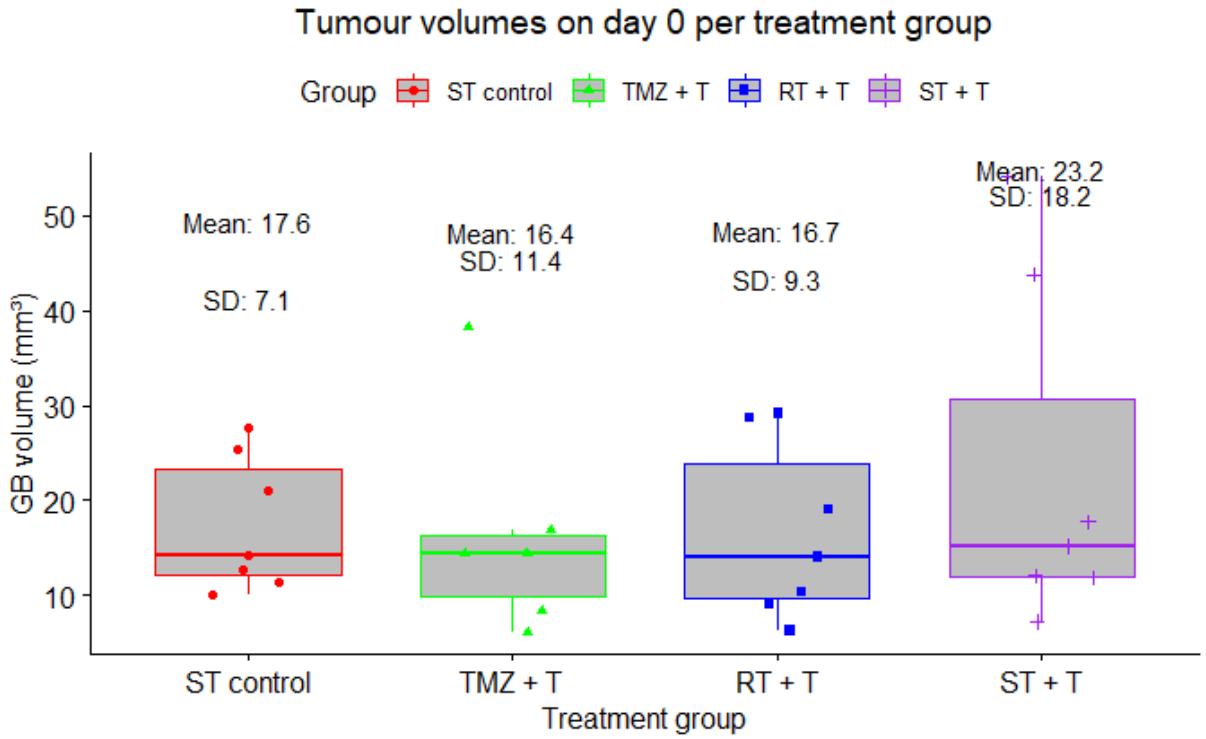

Figure 10: Boxplots of the GB volume on the day of confirmation (i.e. day 0) for each treatment group. ANOVA-analysis resulted in a non-significant (p-value=0,83) difference between the GB tumour volumes on day 0 between the different treatment groups. The mean and SD for each treatment group is depicted. Abbreviations: standard deviation (SD), standard therapy (ST), Temozolomide (TMZ), fractionated radiotherapy (RT), Tonabersat (T).

3.1.2. Effect of Tonabersat on mean GB volume and mean rates of tumour growth

The evolution of the geometric mean tumour volume (mm³) over time for each group is plotted in figure 11A. Table 1 gives an overview of the pairwise comparison between the TMZ + T group and the other treatment groups on day 9, day 12 and day 15. The TMZ + T group showed a rapid proliferation of the GB, leading to euthanasia of all rats within 15 days after GB confirmation (i.e. day 0). The geometric mean tumour volume on day 15 for the TMZ + T group was 206.86 mm³ (SD: 0.91 mm³) (see Table A2 in *Addendum*). A difference in geometric mean GB volume can be observed between the animals from the TMZ + T group and the other

groups (Fig. 11A). This difference is significant on day 12 (p = 0,003 compared with the control group, p = 0,003 compared with the RT + T group, p = 0,009 compared with the ST + T group) and on day 15 (p= 0,0001 compared with the ST control group, p < 0,001 compared with the RT + T and ST+T group). Between the RT + T group, ST + T group and control group no significant differences in geometric mean tumour volumes are observed over time. GB growth was a slower process in these groups, mean tumour volumes comparable with the end point of the mean tumour volumes of the TMZ + T group were reached at day 24 for the control group (geometric mean tumour volume: 202,52 mm³, SD: 34,88 mm³), around day 27 for the ST + T group (geometric mean tumour volume: 240,15 mm³, SD: 22,06 mm³) and at day 30 for the RT + T group (geometric mean tumour volume: 159,7 mm³).

Table A2 (*Addendum*) displays the geometric mean tumour volumes (mm³) for the different time-points for each treatment group with according standard deviation. From day 18 onwards a steep increase in geometric mean volume can be observed for the ST control group, the ST + T group and RT + T group (numbers indicated in red). Based on a visual observation of figure 11A, this steeper increase in geometric mean GB volume for the control group, ST + T and RT + T can also be seen from day 18 onwards. In addition, this is also shown in figure 11B, where the mean rates of tumour growth are plotted. These rates were first standardized through division by the GB volume measured on the day of confirmation (i.e. day 0). The mean rates of tumour growth are shown in table 2. From figure 11B and table 2 it can also be observed that the tumour growth rate of the ST + T is more stable over time compared to the other groups. From day 3 until day 21 it seems that the ST + T group shows a slower tumour progression in comparison to the RT + T group.

CE T1w MRI images of one at random chosen rat of the ST + T group (Fig.12) are added to illustrate that the size of the GB remains visually constant until day 15. From day 18 onwards an increase of tumour volume can be observed. This correlates with what is found in figure 11.

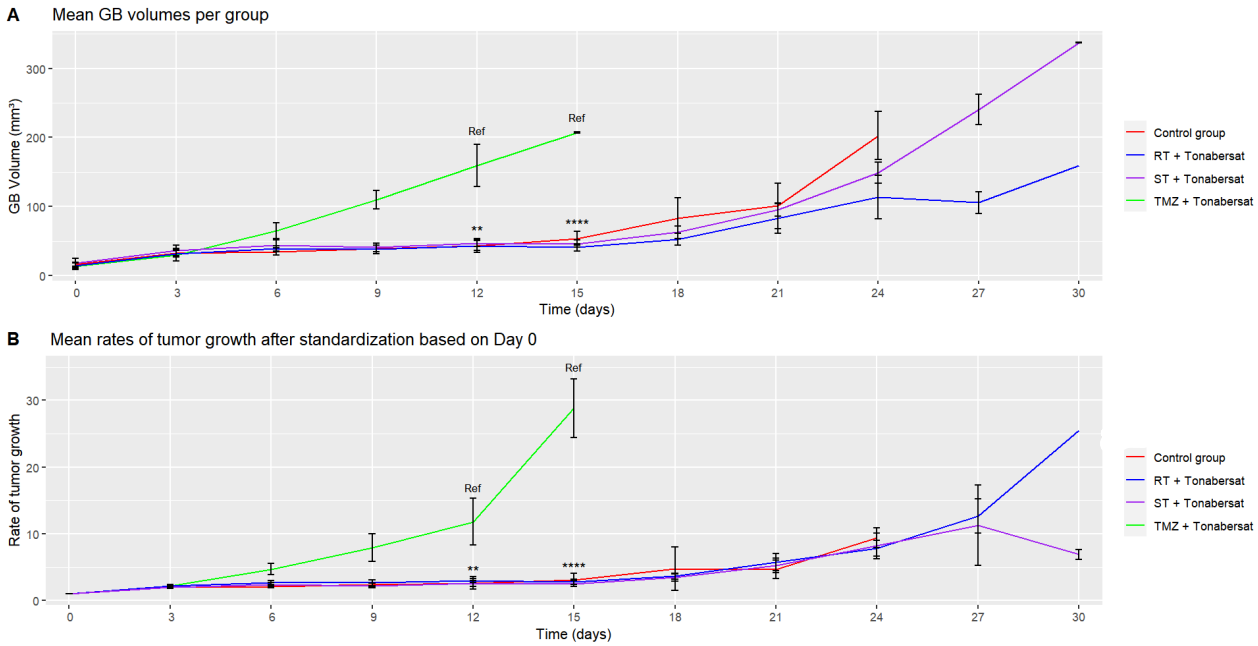

Figure 11: (A) Plot of the geometric mean GB volumes (mm³) per group per time-point. Significant differences between the TMZ + T group (=reference) and RT + T (p = 0,003), control group (p = 0,003) and ST + T (p = 0,009) group are observed on day 12. In addition, on day 15 this difference is significant (p= 0,0001 compared with the control group, p < 0,001 compared with the RT + T and the ST+T group). No significant differences are observed between the RT + T group, ST + T group and ST group.(B) Plot of the mean rates of tumour growth after standardisation based on day of confirmation (i.e. Day 0). The significant differences on day 12 and day 15 are still present. No significant differences are observed between the RT + T group, ST + T group and ST group. Abbreviations: standard therapy (ST), Temozolomide (TMZ), radiotherapy (RT).

	TMZ + T (=reference)		
	D9	D12	D15
ST control	0.16	0.003	0.0001
RT + T	0.13	0.003	<0.0001
ST + T	0.28	0.009	<0.0001

Table 1: Overview of p-values for the comparison between TMZ + T group (=reference) and the ST control group, RT + T group and ST + T group on day 9, day 12 and day 15. P-values in red are significant ($p < 0.05$). Abbreviations: standard therapy (ST), Temozolomide (TMZ), fractionated radiotherapy (RT), Tonabersat (T), day (D).

	ST control	**TMZ + T**	**RT + T**	**ST + T**
	Mean rates of tumour growth + SD	Mean rates of tumour growth + SD	Mean rates of tumour growth + SD	Mean rates of tumour growth + SD
D0	1.000000 (SD: 0.0000000)	1.000000 (SD: 0.0000000)	1.000000 (SD: 0.0000000)	1.000000 (SD: 0.0000000)
D3	2.011114 (SD: 0.1647455)	2.182575 (SD: 0.2230171)	2.201412 (SD: 0.2244318)	1.996216 (SD: 0.1795970)
D6	2.139236 (SD: 0.1978382)	4.712384 (SD: 0.8710184)	2.700572 (SD: 0.3368341)	2.397528 (SD: 0.3071620)
D9	2.382658 (SD: 0.2621757)	7.953949 (SD: 2.0757270)	2.656825 (SD: 0.4193475)	2.240223 (SD: 0.3248482)
D12	2.640553 (SD: 0.9602221)	11.815792 (SD: 3.5202969)	3.012768 (SD: 0.3027746)	2.585238 (SD: 0.4355144)
D15	3.112812 (SD: 0.9722899)	28.814949 (SD: 4.3464081)	2.825313 (SD: 0.4104371)	2.537740 (SD: 0.4067758)
D18	4.793251 (SD: 3.2786918)		3.659187 (SD: 0.4321288)	3.459036 (SD: 0.5469528)
D21	4.698396 (SD: 1.3685043)		5.756419 (SD: 1.2842237)	5.236891 (SD: 1.0747233)
D24	9.425943 (SD: 1.4745613)		7.843389 (SD: 1.1784988)	8.193729 (SD: 1.9219027)
D27			12.650010 (SD: 2.5460273)	11.296346 (SD: 5.9961339)
D30			25.460781	6.919424 (SD: 0.7260687)

Table 2: Overview of the mean rates of tumour growth per time-point per treatment group with according SD. This data was used to create figure 11B. From day 18 onwards a steeper increase can be observed in growth rate (numbers in red) for the ST control group, RT + T group and ST + T group. Abbreviations: standard therapy (ST), Temozolomide (TMZ), fractionated radiotherapy (RT), Tonabersat (T), standard deviation (SD), day (D).

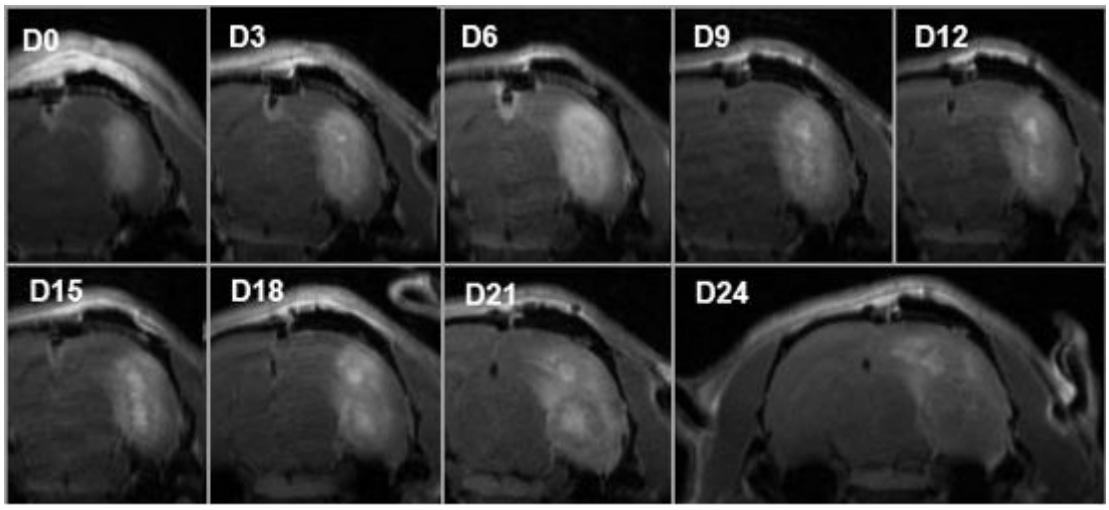

Figure 12: CE-T1W MRI images of one animal of the ST + T group. GB tumour volume stays constant until day 15 and from day 18 onwards an increase in GB volume is observed. Abbreviations: day (D).

3.2. Positive effect of Tonabersat on overall survival

Figure 13 shows the survival probability of each treatment group for different time-points during the experiment. Survival time in this experiment is defined as the time between GB confirmation (i.e. day 0) and humane endpoint. The Kaplan-Meijer survival analysis demonstrates that animals in the ST + T group show the longest survival. These animals live significantly (p = 0,0275) longer compared to the ST control group, which only received RT and TMZ chemotherapy (= reference). Until day 24 all animals of the ST + T group were still alive. The TMZ + T group shows a significant (p = 0,0101) shorter survival in comparison to the ST control group. For the RT + T the difference in overall survival was not significant (p = 0,0971). The results of the pairwise comparison for overall survival can be found in table 3.

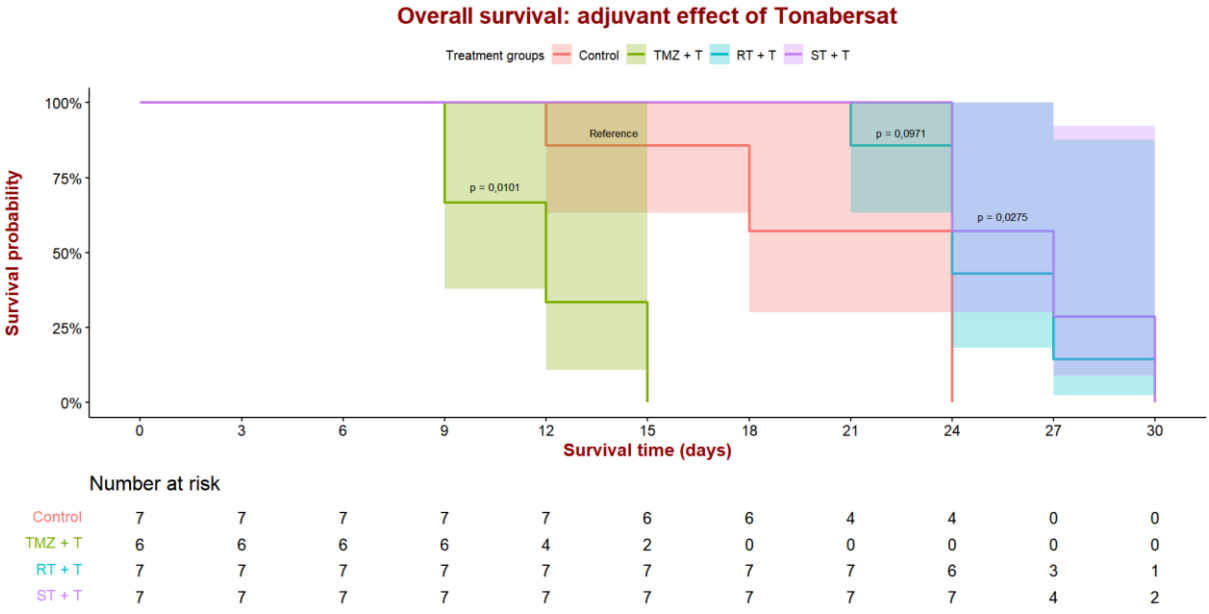

Figure 13: Kaplan-Meijer analysis. A survival curve for each treatment group is shown. For the TMZ + T group a significant decrease (p = 0,0101) in overall survival is observed compared to the control group (=reference). The ST + T group lives significantly longer (p = 0,0275) than the control group. For the RT + T group no difference (p = 0,0971) can be observed compared to the control group. Shaded areas indicate the 95% confidence intervals. Abbreviations: Temozolomide (TMZ), fractionated radiotherapy (RT), Tonaberat (T).

	P-values
ST control group vs. TMZ + T group	0.01011068
ST control group vs. RT + T group	0.09712873
ST control group vs. ST + T group	0.02751051
TMZ + T group vs. RT + T group	0.00188552
TMZ + T group vs. ST + T group	0.00188552
RT + T group vs. ST + T group	0.42301808

Table 3: Overview of p-values for the comparison of the overall survival between all the treatment groups. P-values in red are significant (p<0.005). Abbreviations: standard therapy (ST), Temozolomide (TMZ), fractionated radiotherapy (RT), Tonabersat (T).

The median overall survival time (days) per treatment group is displayed in figure 14. For the TMZ + T group the median overall survival is 12 days. The ST + T group has a median overall survival of 24 days. Both the ST + T group and RT + T group have a median overall survival time of 27 days.

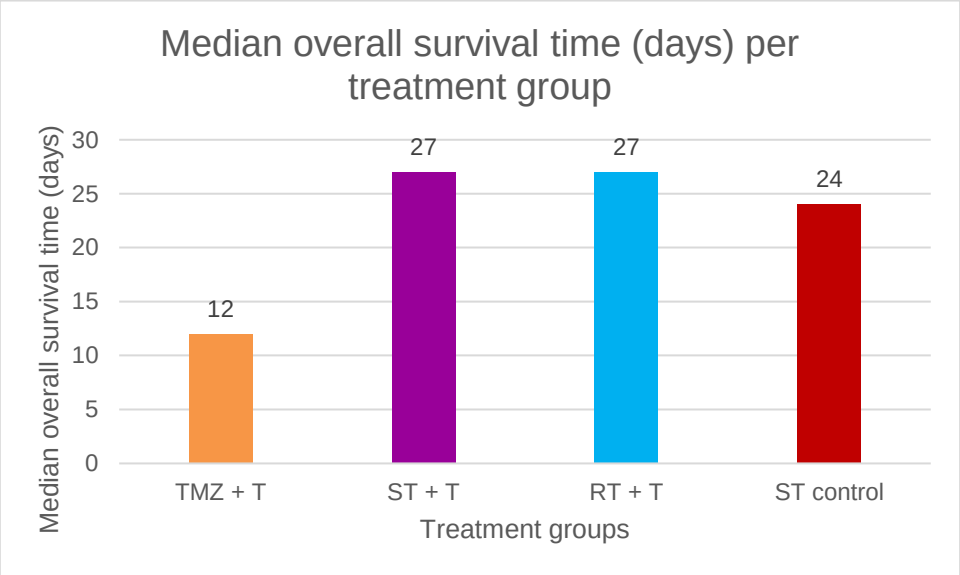

Figure 14: Median overall survival time (days) per treatment group. The median overall survival time for the TMZ + T group is 12 days. For the ST + T group and RT + T group the median overall survival time is 27 days. The median overall survival time for ST control group is 24 days. Abbreviations: standard therapy (ST), Temozolomide (TMZ), fractionated radiotherapy (RT), Tonabersat (T).

3.3. Histological analysis

3.3.1. H&E staining

All the analysed animals showed the presence of a tumour with a necrotic core. The typical histological characteristics of GB include necrosis (a) and a rapid infiltrating growth (b) into the brain parenchyma (c) (Fig.15). These characteristics can be observed on the H&E stained paraffin-embedded slides of the resected brain of an animal of each treatment group. The infiltrative growth is present as small islands of tumour mass in the healthy brain tissue. In addition, microvascular proliferation can be observed on some slices. This confirms the development of GB in the rat brain and demonstrates that the F98 GB rat model closely resembles the human GB.

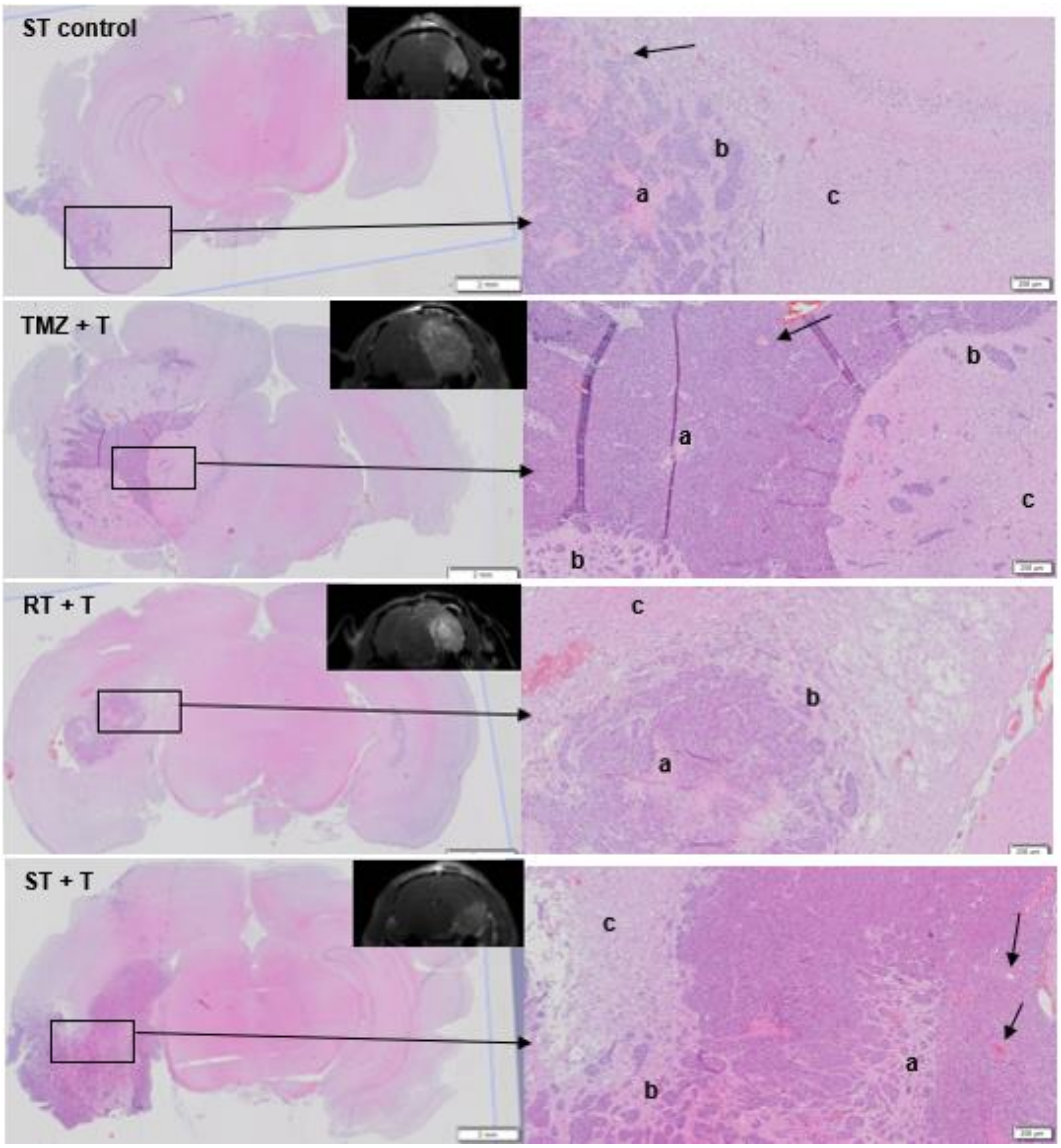

Figure 15: H&E staining of paraffin-embedded brain slices of one animal per treatment group. GB is confirmed with the presence of necrosis (a) and an infiltrating growth (b) into the brain parenchyma (c). Black arrows indicate microvascular proliferation. Scale; left: 2 mm, right: 200µm. Abbreviations: standard therapy (ST), Temozolomide (TMZ), fractionated radiotherapy (RT), Tonabersat (T).

3.3.2. GFAP & Cx43 staining

Reactive astrocytes, which are GFAP positive are present in the peritumoural zone and absent in the tumour tissue (Fig.16). Cx43 expression is also enhanced at the peritumoural zone (Fig.17).

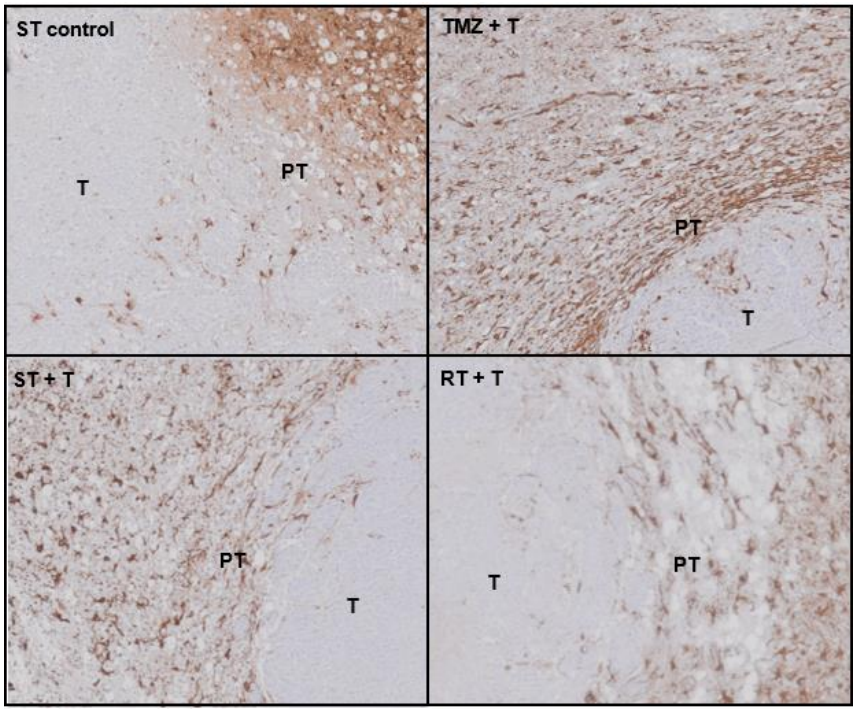

Figure 16: Immunohistochemistry staining for GFAP shows reactive astrocytes peritumourally (PT). No reactive astrocytes are present in the tumour tissue (T). Scale: 100 µm. Abbreviations: standard therapy (ST), Temozolomide (TMZ), fractionated radiotherapy (RT), Tonabersat (T).

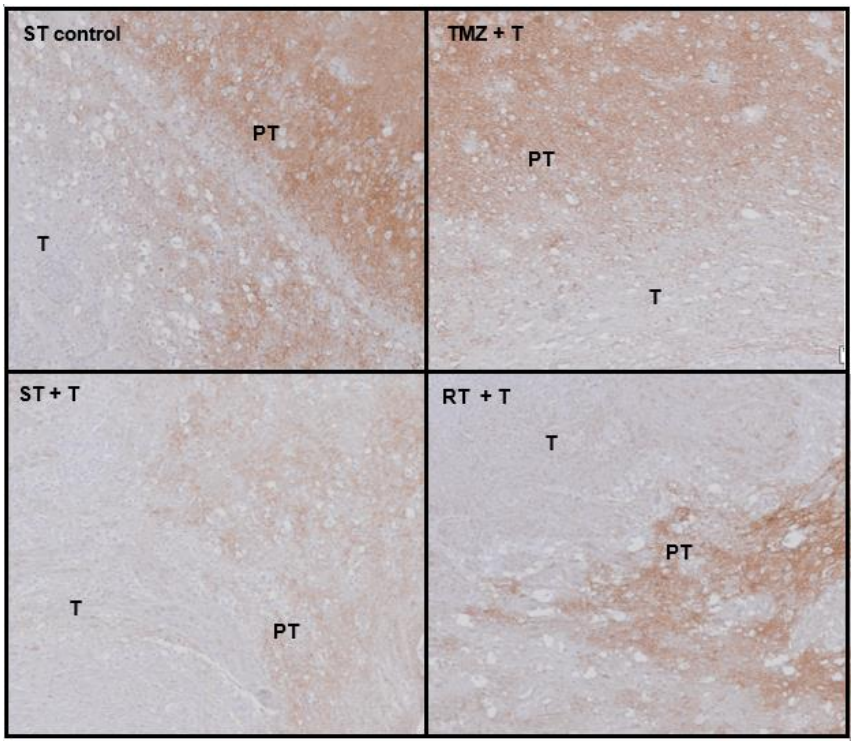

Figure 17: Immunohistochemistry staining for Cx43 shows the absence in the tumour tissue (T) and the presence of Cx43 peritumourally (PT). Scale: 100µm. Abbreviations: standard therapy (ST), Temozolomide (TMZ), fractionated radiotherapy (RT), Tonabersat (T).

4. Discussion

The Stupp protocol is the standard of care for patients with GB since 2005[22]. This protocol consists of radiotherapy and concurrent and adjuvant TMZ chemotherapy, as discussed before. However, the efficacy of this therapy is limited due to overall resistance to the therapy and tumour recurrence. Osswald et al. described the existence of a therapy resistant network connected via TMs composed of Cx43[46]. This network can disperse the radiotherapy-induced increase in intracellular Ca^{2+} concentration, resulting in Ca^{2+} levels that do not induce apoptosis of the GB cells. In addition, several studies have shown that Cx43 has pro-tumourigenic characteristics. Therefore, inhibition of Cx43 GJs may offer new therapeutic strategies. Tonabersat, a Cx43 hemichannel and GJ inhibitor, has already shown its potential to inhibit brain metastasis arising from breast cancer in mouse models[48]. Moreover, Tonabersat has been used in clinical trials regarding the prophylaxis of migraine and is considered safe for application in humans[66].

In our research group De Meulenaere et al. described that the standard medical treatment (TMZ chemotherapy + fractionated radiotherapy) supplemented with Tonabersat was more effective than the standard medical treatment alone[25]. Significant differences between the estimated geometric mean tumour volumes of the standard medical treatment group and standard medical treatment and connexin modulation group were found from day 15 onwards. However, some rats were euthanized because of the development of extra-cranial and/or extra-axial tumours. In our study we used the recently optimised F98 GB rat model in which 5000 F98 cells were inoculated instead of 25000 F98 cells (unpublished results). Limitations regarding the development of extra-cranial and/or extra-axial were not encountered in our experiment. Therefore, all animals were euthanized because of the size of the GB tumour, the development of clinical signs and/or weight loss. During the experiment the rats showed a drop in weight while receiving radiotherapy treatment. The fact that only one animal was euthanized partly due to weight loss (overview of humane endpoints can be found in table A3 of the *Addendum*) shows that the rats are able to recover from the radiotherapy treatment.

Models that represent the human GB are necessary to test new treatments for GB. Our F98 rat model shows all the histological characteristics to consider it as a well-chosen model for this study (fig. 15). The presence of Cx43 at the peritumoural zone was already demonstrated by De Meulenaere et al[25]. Our Cx43 immunohistochemistry staining confirms this observation (fig.17). The presence of Cx43 is important in this study as inhibition of Cx43 cannot take place if Cx43 is not expressed. From the histological analysis we can conclude that we have a good GB model with presence of Cx43, resulting in reliable results.

Our study results indicate that addition of Tonabersat to the standard therapy leads to a prolonged survival time. A Kaplan-Meijer analysis demonstrated that the animals of the ST + T and RT + T group live approximately six days longer than the ST control group. However, the difference in survival time between the control group and the RT + T group was not significant, while the difference between the control group and ST + T group was significant (Fig. 13, table 2). In contrast, the combination of TMZ chemotherapy and Tonabersat results in a significant shorter lifespan in comparison to the control group. A study of Yusubalieva et al., which was previously discussed, also resulted in a prolonging of the survival time when a monoclonal antibody targeting Cx43 was combined with radiotherapy in the C6 rat model, while combination of TMZ chemotherapy and the antibody abolished the antitumour effect, resulting in a shorter lifespan of the rats[57,58].

Stupp et al. already demonstrated that addition of TMZ chemotherapy to radiotherapy leads to an increase in overall survival from 12 to 14 months[22]. TMZ is considered a radiosensitizer, meaning that it makes the cells more sensitive to radiotherapy and thus improves the efficacy of radiotherapy[101,102]. Since the difference in mean rates of tumour growth between the ST + T group and RT + T group is negligible (Fig. 11B), it can be assumed that TMZ and Tonabersat have the same mechanism of action. Our study results suggest that Tonabersat is a

radiosensitizer. It makes the GB cells more sensitive to radiotherapy, thus making radiotherapy an essential part of the treatment strategy. This can explain the shorter lifespan of the TMZ + T group and the rapid proliferation in this group, because there is no radiotherapy-induced apoptosis of the GB cells. A hypothesis for this radiosensitization might be that by blocking Cx43, a disconnection of the therapy resistant network occurs and lethal levels of radiotherapy-induced Ca^{2+} can be achieved, resulting in GB cell death. Moreover, it has been observed that fractionated radiotherapy can increase BBB permeability to biological macromolecules in C6 glioma[103]. This can improve the drug delivery to the brain, and might allow Tonabersat to reach the tumour more easily.

The prolonged survival time might also be due to the fact that addition of Tonabersat to RT or ST leads to less infiltration into the brain parenchyma. Inhibition of Cx43 with the use of Tonabersat reduces the invasion of GB cells into the healthy brain tissue. Our histological analysis confirmed the presence of GFAP-positive astrocytes and Cx43 at the tumour border, reflecting that Tonabersat might be active at the tumour border (Fig. 11 & 12). Our study results correlate with the findings of McCutheon et al. and Sin et al., who showed that deletion of Cx43 reduces the invasive capacity of GB[45,47]. Bates et al. obtained similar results by downregulation of Cx43 with the use of RNAi, as mentioned earlier[52].

In addition, chemoresistance is a frequent occurring phenomenon in GB, with only 40% of patients being chemosensitive because of MGMT promotor methylation[24]. Chen et al. demonstrated that co-culture of glioma cells with human astrocytes resulted in a decreased apoptosis of glioma cells induced by TMZ chemotherapy[104]. They suggested that Cx43 controls the cytoplasmic calcium level through Cx43 GJs, resulting in protection from the chemotherapeutic drugs. When a GJ inhibitor was added to this co-culture, this protection was lost. Additionally, Murphy et al. sensitized human MGMT-deficient and TMZ-resistant GB cells to TMZ chemotherapy by using αCT1, an inhibitor of Cx43, as mentioned earlier[59]. This indicates that Cx43 renders GB cells resistant to TMZ. In our experiment Cx43 is inhibited by Tonabersat intratumourally as well as between GB cells and astrocytes. This suggests that the TMZ chemoresistance is decreased, resulting in a decrease in tumour regrowth. However, treatment with TMZ chemotherapy in combination with Tonabersat does not have an effect on overall survival and geometric mean GB volumes (Fig. 11 & Fig. 13). This treatment group did not receive radiotherapy, suggesting again that Tonabersat might be radiosensitive and radiotherapy is needed for a proper functioning of Tonabersat. Since no radiotherapy was administered in the TMZ + T group, Tonabersat could not exert its function. Less tumour regrowth indicates that the tumour is less aggressive resulting in a prolonged survival time. This can also explain why the ST + T group, which received TMZ chemotherapy, shows a more stable progression in mean tumour growth rate over time in comparison to the control and RT + T group, which did not receive TMZ chemotherapy (Table 2).

On the day of confirmation (i.e. day 0) the geometric mean GB volumes of the treatment groups did not differ significantly from each other (Fig. 10). This implies that no animal started the experiment with an already enlarged tumour size. No significant differences in geometric mean tumour growth rates (Fig. 11B) between the control group, RT + T and ST + T group can be observed at all the time-points. The growth rate of these treatment groups stays stable until day 15, from day 18 onwards a steep increase can be observed (Table 2). There is no change in tumour growth rate when Tonabersat is added to the treatment, but there is a significant difference in survival time. This shows the conflicting roles of Cx43 in GB; Cx43 is considered both a tumour suppressor and tumour promotor[105]. During the initial growth of the tumour, Cx43 has a tumour suppressive role. During tumour infiltration, Cx43 has a more tumour promoting role. Cx43 is considered as a negative regulator of cell growth[56]. A study using Tolbutamide, which increases the synthesis of Cx43, resulted in a reduction of C6-glioma cell proliferation[106]. Thus inhibition of Cx43 by Tonabersat might not result in a reduction of glioma cell proliferation. In addition, in the GB tumour core there is almost no expression of Cx43 (Fig.17), indicating that Tonabersat mainly exerts its function at the tumour border.

To conclude, these study results indicate that Tonabersat has therapeutic potential when added to the standard medical treatment (fractionated RT and TMZ chemotherapy) or radiotherapy treatment. The standard medical treatment or radiotherapy supplemented with Tonabersat results in a prolonging of the survival time. We suggest that the necessity of radiotherapy indicates that Tonabersat might be radiosensitive. The tumour growth rates are not significantly affected when Tonabersat is added to the therapy, this might indicate that inhibition of Cx43 does not inhibit the capacity of tumour growth. More research needs to be conducted to confirm these findings.

5. Reference list

1 Jessen, K. R. Glial cells. *Int J Biochem Cell Biol* **36**, 1861-1867, doi:10.1016/j.biocel.2004.02.023 (2004).

2 He, F. & Sun, Y. E. Glial cells more than support cells? *Int J Biochem Cell Biol* **39**, 661-665, doi:10.1016/j.biocel.2006.10.022 (2007).

3 Azevedo, F. A. C. *et al.* Equal numbers of neuronal and nonneuronal cells make the human brain an isometrically scaled-up primate brain. *Journal of Comparative Neurology* **513**, 532-541, doi:https://doi.org/10.1002/cne.21974 (2009).

4 Lovinger, D. M. Communication networks in the brain: neurons, receptors, neurotransmitters, and alcohol. *Alcohol Res Health* **31**, 196-214 (2008).

5 Da Ros, M. *et al.* Glioblastoma Chemoresistance: The Double Play by Microenvironment and Blood-Brain Barrier. *Int J Mol Sci* **19**, doi:10.3390/ijms19102879 (2018).

6 Daneman, R. & Prat, A. The blood-brain barrier. *Cold Spring Harb Perspect Biol* **7**, a020412, doi:10.1101/cshperspect.a020412 (2015).

7 Abbott, N. J., Patabendige, A. A., Dolman, D. E., Yusof, S. R. & Begley, D. J. Structure and function of the blood-brain barrier. *Neurobiol Dis* **37**, 13-25, doi:10.1016/j.nbd.2009.07.030 (2010).

8 Lochhead, J. J., Yang, J., Ronaldson, P. T. & Davis, T. P. Structure, Function, and Regulation of the Blood-Brain Barrier Tight Junction in Central Nervous System Disorders. *Front Physiol* **11**, 914, doi:10.3389/fphys.2020.00914 (2020).

9 Weller, M. *et al.* Glioma. *Nat Rev Dis Primers* **1**, 15017, doi:10.1038/nrdp.2015.17 (2015).

10 Jiang, Y. & Uhrbom, L. On the origin of glioma. *Upsala Journal of Medical Sciences* **117**, 113-121, doi:10.3109/03009734.2012.658976 (2012).

11 Crivii, C. B. *et al.* Glioblastoma Microenvironment and Cellular Interactions. *Cancers* **14**, doi:10.3390/cancers14041092 (2022).

12 Zong, H., Verhaak, R. G. W. & Canoll, P. The cellular origin for malignant glioma and prospects for clinical advancements. *Expert Review of Molecular Diagnostics* **12**, 383-394, doi:10.1586/erm.12.30 (2012).

13 Louis, D. N. *et al.* The 2007 WHO classification of tumours of the central nervous system. *Acta neuropathologica* **114**, 97-109, doi:10.1007/s00401-007-0243-4 (2007).

14 Gritsch, S., Batchelor, T. T. & Gonzalez Castro, L. N. Diagnostic, therapeutic, and prognostic implications of the 2021 World Health Organization classification of tumors of the central nervous system. *Cancer* **128**, 47-58, doi:10.1002/cncr.33918 (2022).

15 Louis, D. N. *et al.* The 2021 WHO Classification of Tumors of the Central Nervous System: a summary. *Neuro Oncol* **23**, 1231-1251, doi:10.1093/neuonc/noab106 (2021).

16 Watanabe, K. *et al.* Overexpression of the EGF receptor and p53 mutations are mutually exclusive in the evolution of primary and secondary glioblastomas. *Brain Pathol* **6**, 217-223; discussion 223-214, doi:10.1111/j.1750-3639.1996.tb00848.x (1996).

17 Ohgaki, H. & Kleihues, P. The definition of primary and secondary glioblastoma. *Clin Cancer Res* **19**, 764-772, doi:10.1158/1078-0432.Ccr-12-3002 (2013).

18 Wirsching, H. G., Galanis, E. & Weller, M. Glioblastoma. *Handb Clin Neurol* **134**, 381-397, doi:10.1016/b978-0-12-802997-8.00023-2 (2016).

19 Guan, X., Hasan, M. N., Maniar, S., Jia, W. & Sun, D. Reactive Astrocytes in Glioblastoma Multiforme. *Molecular Neurobiology* **55**, 6927-6938, doi:10.1007/s12035-018-0880-8 (2018).

20 Omuro, A. & DeAngelis, L. M. Glioblastoma and other malignant gliomas: a clinical review. *Jama* **310**, 1842-1850, doi:10.1001/jama.2013.280319 (2013).

21 Fernandes, C. *et al.* in *Glioblastoma* (ed S. De Vleeschouwer) (Codon Publications

Copyright: The Authors., 2017).

22 Stupp, R. *et al.* Radiotherapy plus Concomitant and Adjuvant Temozolomide for Glioblastoma. *New England Journal of Medicine* **352**, 987-996, doi:10.1056/NEJMoa043330 (2005).

23 Friedman, H. S., Kerby, T. & Calvert, H. Temozolomide and Treatment of Malignant Glioma1. *Clinical Cancer Research* **6**, 2585-2597 (2000).

24 Aldape, K., Zadeh, G., Mansouri, S., Reifenberger, G. & von Deimling, A. Glioblastoma: pathology, molecular mechanisms and markers. *Acta neuropathologica* **129**, 829-848, doi:10.1007/s00401-015-1432-1 (2015).

25 De Meulenaere, V. *et al.* Adjuvant therapeutic potential of tonabersat in the standard treatment of glioblastoma: A preclinical F98 glioblastoma rat model study. *PLoS One* **14**, e0224130, doi:10.1371/journal.pone.0224130 (2019).

26 Schneider, M. R. & Wolf, E. The epidermal growth factor receptor ligands at a glance. *J Cell Physiol* **218**, 460-466, doi:https://doi.org/10.1002/jcp.21635 (2009).
27 Talasila, K. M. *et al.* EGFR wild-type amplification and activation promote invasion and development of glioblastoma independent of angiogenesis. *Acta Neuropathologica* **125**, 683-698, doi:10.1007/s00401-013-1101-1 (2013).
28 McNamara, M. G., Sahebjam, S. & Mason, W. P. Emerging biomarkers in glioblastoma. *Cancers* **5**, 1103-1119, doi:10.3390/cancers5031103 (2013).
29 Simon, M. *et al.* TERT promoter mutations: a novel independent prognostic factor in primary glioblastomas. *Neuro Oncol* **17**, 45-52, doi:10.1093/neuonc/nou158 (2015).
30 Arslantas, A. *et al.* Genomic alterations in low-grade, anaplastic astrocytomas and glioblastomas. *Pathology & Oncology Research* **13**, 39-46, doi:10.1007/BF02893439 (2007).
31 Parsons, D. W. *et al.* An Integrated Genomic Analysis of Human Glioblastoma Multiforme. *Science* **321**, 1807-1812, doi:doi:10.1126/science.1164382 (2008).
32 Brandao, M., Simon, T., Critchley, G. & Giamas, G. Astrocytes, the rising stars of the glioblastoma microenvironment. *Glia* **67**, 779-790, doi:10.1002/glia.23520 (2019).
33 Buonfiglioli, A. & Hambardzumyan, D. Macrophages and microglia: the cerberus of glioblastoma. *Acta Neuropathologica Communications* **9**, 54, doi:10.1186/s40478-021-01156-z (2021).
34 Quail, D. F. & Joyce, J. A. The Microenvironmental Landscape of Brain Tumors. *Cancer Cell* **31**, 326-341, doi:10.1016/j.ccell.2017.02.009 (2017).
35 Hambardzumyan, D. & Bergers, G. Glioblastoma: Defining Tumor Niches. *Trends Cancer* **1**, 252-265, doi:10.1016/j.trecan.2015.10.009 (2015).
36 Dapash, M., Hou, D., Castro, B., Lee-Chang, C. & Lesniak, M. S. The Interplay between Glioblastoma and Its Microenvironment. *Cells* **10**, doi:10.3390/cells10092257 (2021).
37 Schiffer, D. *et al.* Glioblastoma niches: from the concept to the phenotypical reality. *Neurol Sci* **39**, 1161-1168, doi:10.1007/s10072-018-3408-0 (2018).
38 Biserova, K., Jakovlevs, A., Uljanovs, R. & Strumfa, I. Cancer Stem Cells: Significance in Origin, Pathogenesis and Treatment of Glioblastoma. *Cells* **10**, doi:10.3390/cells10030621 (2021).
39 Kucharzewska, P., Christianson, H. C. & Belting, M. Global profiling of metabolic adaptation to hypoxic stress in human glioblastoma cells. *PLoS One* **10**, e0116740, doi:10.1371/journal.pone.0116740 (2015).
40 Sáez, J. C., Contreras, J. E., Bukauskas, F. F., Retamal, M. A. & Bennett, M. V. L. Gap junction hemichannels in astrocytes of the CNS. *Acta Physiologica Scandinavica* **179**, 9-22, doi:https://doi.org/10.1046/j.1365-201X.2003.01196.x (2003).
41 Juan, A. O. in *Glia in Health and Disease* (ed Spohr Tania) Ch. 1 (IntechOpen, 2019).
42 Spray, D. C., Ye, Z.-C. & Ransom, B. R. Functional connexin "hemichannels": A critical appraisal. *Glia* **54**, 758-773, doi:https://doi.org/10.1002/glia.20429 (2006).
43 Aasen, T. *et al.* Connexins in cancer: bridging the gap to the clinic. *Oncogene* **38**, 4429-4451, doi:10.1038/s41388-019-0741-6 (2019).
44 Crespin, S. *et al.* Expression of a gap junction protein, connexin43, in a large panel of human gliomas: new insights. *Cancer Med* **5**, 1742-1752, doi:10.1002/cam4.730 (2016).
45 McCutcheon, S. & Spray, D. C. Glioblastoma-Astrocyte Connexin 43 Gap Junctions Promote Tumor Invasion. *Mol Cancer Res* **20**, 319-331, doi:10.1158/1541-7786.Mcr-21-0199 (2022).
46 Osswald, M. *et al.* Brain tumour cells interconnect to a functional and resistant network. *Nature* **528**, 93-98, doi:10.1038/nature16071 (2015).
47 Sin, W. C. *et al.* Astrocytes promote glioma invasion via the gap junction protein connexin43. *Oncogene* **35**, 1504-1516, doi:10.1038/onc.2015.210 (2016).
48 Chen, Q. *et al.* Carcinoma-astrocyte gap junctions promote brain metastasis by cGAMP transfer. *Nature* **533**, 493-498, doi:10.1038/nature18268 (2016).
49 Ferraro, G. B., Kodack, D. P., Askoxylakis, V. & Jain, R. K. Closing the gap: astrocytes and brain metastasis. *Cell Research* **26**, 973-974, doi:10.1038/cr.2016.96 (2016).
50 Tombal, B., Denmeade, S. R., Gillis, J. M. & Isaacs, J. T. A supramicromolar elevation of intracellular free calcium ([Ca(2+)](i)) is consistently required to induce the execution phase of apoptosis. *Cell Death Differ* **9**, 561-573, doi:10.1038/sj.cdd.4400999 (2002).
51 Malkki, H. Astrocytoma cells interconnect to resist radiotherapy. *Nature Reviews Clinical Oncology* **13**, 3-3, doi:10.1038/nrclinonc.2015.214 (2016).
52 Bates, D. C., Sin, W. C., Aftab, Q. & Naus, C. C. Connexin43 enhances glioma invasion by a mechanism involving the carboxy terminus. *Glia* **55**, 1554-1564, doi:https://doi.org/10.1002/glia.20569 (2007).

53 Aftab, Q., Sin, W. C. & Naus, C. C. Reduction in gap junction intercellular communication promotes glioma migration. *Oncotarget* **6**, 11447-11464, doi:10.18632/oncotarget.3407 (2015).
54 Hong, X., Sin, W. C., Harris, A. L. & Naus, C. C. Gap junctions modulate glioma invasion by direct transfer of microRNA. *Oncotarget* **6**, 15566-15577, doi:10.18632/oncotarget.3904 (2015).
55 Uzu, M., Sin, W. C., Shimizu, A. & Sato, H. Conflicting Roles of Connexin43 in Tumor Invasion and Growth in the Central Nervous System. *Int J Mol Sci* **19**, doi:10.3390/ijms19041159 (2018).
56 Sin, W. C., Crespin, S. & Mesnil, M. Opposing roles of connexin43 in glioma progression. *Biochim Biophys Acta* **1818**, 2058-2067, doi:10.1016/j.bbamem.2011.10.022 (2012).
57 Yusubalieva, G. M. *et al.* Antitumor effects of monoclonal antibodies to connexin 43 extracellular fragment in induced low-differentiated glioma. *Bull Exp Biol Med* **153**, 163-169, doi:10.1007/s10517-012-1667-y (2012).
58 Yusubalieva, G. M. *et al.* Treatment of poorly differentiated glioma using a combination of monoclonal antibodies to extracellular connexin-43 fragment, temozolomide, and radiotherapy. *Bull Exp Biol Med* **157**, 510-515, doi:10.1007/s10517-014-2603-0 (2014).
59 Murphy, S. F. *et al.* Connexin 43 Inhibition Sensitizes Chemoresistant Glioblastoma Cells to Temozolomide. *Cancer Res* **76**, 139-149, doi:10.1158/0008-5472.Can-15-1286 (2016).
60 Gielen, P. R. *et al.* Connexin43 confers Temozolomide resistance in human glioma cells by modulating the mitochondrial apoptosis pathway. *Neuropharmacology* **75**, 539-548, doi:10.1016/j.neuropharm.2013.05.002 (2013).
61 Pridham, K. J. *et al.* Connexin 43 confers chemoresistance through activating PI3K. *Oncogenesis* **11**, 2, doi:10.1038/s41389-022-00378-7 (2022).
62 Kim, Y. *et al.* Tonabersat Prevents Inflammatory Damage in the Central Nervous System by Blocking Connexin43 Hemichannels. *Neurotherapeutics* **14**, 1148-1165, doi:10.1007/s13311-017-0536-9 (2017).
63 Mugisho, O. O. *et al.* The inflammasome pathway is amplified and perpetuated in an autocrine manner through connexin43 hemichannel mediated ATP release. *Biochim Biophys Acta Gen Subj* **1862**, 385-393, doi:10.1016/j.bbagen.2017.11.015 (2018).
64 Lyon, H., Shome, A., Rupenthal, I. D., Green, C. R. & Mugisho, O. O. Tonabersat Inhibits Connexin43 Hemichannel Opening and Inflammasome Activation in an In Vitro Retinal Epithelial Cell Model of Diabetic Retinopathy. *Int J Mol Sci* **22**, doi:10.3390/ijms22010298 (2020).
65 Chan, W. N. *et al.* Identification of (−)-cis-6-acetyl-4S-(3-chloro-4-fluoro-benzoylamino)-3,4-dihydro-2,2-dimethyl-2H-benzo[b]pyran-3S-ol as a potential antimigraine agent. *Bioorganic & Medicinal Chemistry Letters* **9**, 285-290, doi:https://doi.org/10.1016/S0960-894X(98)00728-8 (1999).
66 Hauge, A. W., Asghar, M. S., Schytz, H. W., Christensen, K. & Olesen, J. Effects of tonabersat on migraine with aura: a randomised, double-blind, placebo-controlled crossover study. *Lancet Neurol* **8**, 718-723, doi:10.1016/s1474-4422(09)70135-8 (2009).
67 Borsook, D., Maleki, N. & Burstein, R. in *Neurobiology of Brain Disorders* (eds Michael J. Zigmond, Lewis P. Rowland, & Joseph T. Coyle) 693-708 (Academic Press, 2015).
68 Li, Q. *et al.* Targeting gap junction in epilepsy: Perspectives and challenges. *Biomedicine & Pharmacotherapy* **109**, 57-65, doi:https://doi.org/10.1016/j.biopha.2018.10.068 (2019).
69 Blower, P., White, H. & Elrod, S. Tonabersat, a Novel Investigational Anti-Seizure Drug, Inhibits Seizures in Models of Generalized Epilepsy (P02.209). *Neurology* **80**, P02.209-P202.209 (2013).
70 Kurokawa, T., Kazuta, Y. & Watanabe, T. in *Comprehensive Medicinal Chemistry III* (eds Samuel Chackalamannil, David Rotella, & Simon E. Ward) 1-19 (Elsevier, 2017).
71 Sharma, H. A. MRI physics–basic principles. *Acta Neuropsychiatrica* **21**, 200-201, doi:10.1111/j.1601-5215.2009.00404.x (2009).
72 Plewes, D. B. & Kucharczyk, W. Physics of MRI: a primer. *J Magn Reson Imaging* **35**, 1038-1054, doi:10.1002/jmri.23642 (2012).
73 Currie, S., Hoggard, N., Craven, I. J., Hadjivassiliou, M. & Wilkinson, I. D. Understanding MRI: basic MR physics for physicians. *Postgrad Med J* **89**, 209-223, doi:10.1136/postgradmedj-2012-131342 (2013).
74 van Geuns, R.-J. M. *et al.* Basic principles of magnetic resonance imaging. *Progress in Cardiovascular Diseases* **42**, 149-156, doi:https://doi.org/10.1016/S0033-0620(99)70014-9 (1999).
75 Serai, S. D., Ho, M. L., Artunduaga, M., Chan, S. S. & Chavhan, G. B. Components of a magnetic resonance imaging system and their relationship to safety and image quality. *Pediatr Radiol* **51**, 716-723, doi:10.1007/s00247-020-04894-9 (2021).

76 Delso, G., Ter Voert, E. & Veit-Haibach, P. How does PET/MR work? Basic physics for physicians. *Abdom Imaging* **40**, 1352-1357, doi:10.1007/s00261-015-0437-5 (2015).

77 Budinger, T. F. & Bird, M. D. MRI and MRS of the human brain at magnetic fields of 14T to 20T: Technical feasibility, safety, and neuroscience horizons. *NeuroImage* **168**, 509-531, doi:https://doi.org/10.1016/j.neuroimage.2017.01.067 (2018).

78 Xiao, Y. D. *et al.* MRI contrast agents: Classification and application (Review). *Int J Mol Med* **38**, 1319-1326, doi:10.3892/ijmm.2016.2744 (2016).

79 Wahsner, J., Gale, E. M., Rodríguez-Rodríguez, A. & Caravan, P. Chemistry of MRI Contrast Agents: Current Challenges and New Frontiers. *Chemical Reviews* **119**, 957-1057, doi:10.1021/acs.chemrev.8b00363 (2019).

80 Chen, C. *et al.* Ultrasmall superparamagnetic iron oxide nanoparticles: A next generation contrast agent for magnetic resonance imaging. *WIREs Nanomedicine and Nanobiotechnology* **14**, e1740, doi:https://doi.org/10.1002/wnan.1740 (2022).

81 Blomqvist, L., Nordberg, G. F., Nurchi, V. M. & Aaseth, J. O. Gadolinium in Medical Imaging—Usefulness, Toxic Reactions and Possible Countermeasures—A Review. *Biomolecules* **12**, 742 (2022).

82 Sorensen, A. G., Tievsky, A. L., Ostergaard, L., Weisskoff, R. M. & Rosen, B. R. Contrast agents in functional MR imaging. *Journal of Magnetic Resonance Imaging* **7**, 47-55, doi:https://doi.org/10.1002/jmri.1880070108 (1997).

83 Pope, W. B. & Brandal, G. Conventional and advanced magnetic resonance imaging in patients with high-grade glioma. *Q J Nucl Med* **62**, 239-253, doi:10.23736/s1824-4785.18.03086-8 (2018).

84 Shukla, G. *et al.* Advanced magnetic resonance imaging in glioblastoma: a review. *Chin Clin Oncol* **6**, 40, doi:10.21037/cco.2017.06.28 (2017).

85 Lenting, K., Verhaak, R., ter Laan, M., Wesseling, P. & Leenders, W. Glioma: experimental models and reality. *Acta Neuropathologica* **133**, 263-282, doi:10.1007/s00401-017-1671-4 (2017).

86 HICKS, W. H. *et al.* Large Animal Models of Glioma: Current Status and Future Prospects. *Anticancer Research* **41**, 5343-5353, doi:10.21873/anticanres.15347 (2021).

87 Liu, P. *et al.* Preclinical models of glioblastoma: limitations of current models and the promise of new developments. *Expert Rev Mol Med* **23**, e20, doi:10.1017/erm.2021.20 (2021).

88 Robertson, F. L., Marqués-Torrejón, M.-A., Morrison, G. M. & Pollard, S. M. Experimental models and tools to tackle glioblastoma. *Disease Models & Mechanisms* **12**, doi:10.1242/dmm.040386 (2019).

89 Sahu, U., Barth, R. F., Otani, Y., McCormack, R. & Kaur, B. Rat and Mouse Brain Tumor Models for Experimental Neuro-Oncology Research. *J Neuropathol Exp Neurol* **81**, 312-329, doi:10.1093/jnen/nlac021 (2022).

90 Jacobs, V. L., Valdes, P. A., Hickey, W. F. & De Leo, J. A. Current Review of in Vivo GBM Rodent Models: Emphasis on the CNS-1 Tumour Model. *ASN Neuro* **3**, AN20110014, doi:10.1042/an20110014 (2011).

91 Szadvari, I., Krizanova, O. & Babula, P. Athymic nude mice as an experimental model for cancer treatment. *Physiol Res* **65**, S441-s453, doi:10.33549/physiolres.933526 (2016).

92 Vanhove, C. & Goethals, I. Magnetic resonance imaging-guided radiation therapy using animal models of glioblastoma. *The British Journal of Radiology* **92**, 20180713, doi:10.1259/bjr.20180713 (2019).

93 Shahzad, U. *et al.* Modeling human brain tumors in flies, worms, and zebrafish: From proof of principle to novel therapeutic targets. *Neuro Oncol* **23**, 718-731, doi:10.1093/neuonc/noaa306 (2021).

94 Herranz, C. *et al.* Spontaneously Arising Canine Glioma as a Potential Model for Human Glioma. *Journal of Comparative Pathology* **154**, 169-179, doi:https://doi.org/10.1016/j.jcpa.2015.12.001 (2016).

95 Tong, Y. *et al.* A tree shrew glioblastoma model recapitulates features of human glioblastoma. *Oncotarget* **8**, 17897-17907, doi:10.18632/oncotarget.15225 (2017).

96 Brockmann, M. A. Use of clinical MR scanners for small rodent imaging. *Methods* **43**, 1, doi:https://doi.org/10.1016/j.ymeth.2007.08.002 (2007).

97 Denic, A. *et al.* MRI in rodent models of brain disorders. *Neurotherapeutics* **8**, 3-18, doi:10.1007/s13311-010-0002-4 (2011).

98 Lauber, D. T. *et al.* State of the art in vivo imaging techniques for laboratory animals. *Lab Anim* **51**, 465-478, doi:10.1177/0023677217695852 (2017).

99 Hoyer, C., Gass, N., Weber-Fahr, W. & Sartorius, A. Advantages and challenges of small animal magnetic resonance imaging as a translational tool. *Neuropsychobiology* **69**, 187-201, doi:10.1159/000360859 (2014).
100 Bouckaert, C. *et al.* Development of a Rat Model for Glioma-Related Epilepsy. *Int J Mol Sci* **21**, doi:10.3390/ijms21196999 (2020).
101 Babaloui, S. *et al.* Radiosensitization of Glioma Cells by Temozolomide (TMZ): A Colony Formation Assay. *J Biomed Phys Eng* **12**, 43-50, doi:10.31661/jbpe.v0i0.1223 (2022).
102 Borhani, S., Mozdarani, H., Babalui, S., Bakhshandeh, M. & Nosrati, H. In Vitro Radiosensitizing Effects of Temozolomide on U87MG Cell Lines of Human Glioblastoma Multiforme. *Iran J Med Sci* **42**, 258-265 (2017).
103 Yusubalieva, G. M. *et al.* Blood-brain barrier permeability in healthy rats and rats with experimental C6 glioma after fractionated radiotherapy of the brain. *Zh Vopr Neirokhir Im N N Burdenko* **79**, 15-26, doi:10.17116/neiro201579315-26 (2015).
104 Chen, W. *et al.* Glioma cells escaped from cytotoxicity of temozolomide and vincristine by communicating with human astrocytes. *Med Oncol* **32**, 43, doi:10.1007/s12032-015-0487-0 (2015).
105 Sin, W.-C., Crespin, S. & Mesnil, M. Opposing roles of connexin43 in glioma progression. *Biochimica et Biophysica Acta (BBA) - Biomembranes* **1818**, 2058-2067, doi:https://doi.org/10.1016/j.bbamem.2011.10.022 (2012).
106 Sánchez-Alvarez, R., Paíno, T., Herrero-González, S., Medina, J. M. & Tabernero, A. Tolbutamide reduces glioma cell proliferation by increasing connexin43, which promotes the up-regulation of p21 and p27 and subsequent changes in retinoblastoma phosphorylation. *Glia* **54**, 125-134, doi:10.1002/glia.20363 (2006).

Poster

FACULTY OF MEDICINE AND HEALTH SCIENCES
infinity
GHENT UNIVERSITY

ketelaere Ellen | Prof. Dr. Karel Deblaere | Dr. Valerie De Meulenaere | Velislava Zoteva

DEPARTMENT OF DIAGNOSTIC SCIENCES

INVESTIGATING THE THERAPEUTIC POTENTIAL OF TONABERSAT FOR THE TREATMENT OF GB USING THE F98 GB RAT MODEL

GLIOBLASTOMA

= grade IV astrocytoma

- 46% or primary malignant brain tumours
- Arise from glial cells
- Diagnosis: MRI
- 5-year survival rate 5%
- Current treatment:

Surgery | Radiotherapy | Chemotherapy

→ Limited efficacy due to overall resistance

CONNEXIN 43 & TONABERSAT

- Cx43 found in over 60% of GBs
- Cx43 has a role in cancer pathogenesis

→ Cx43-based gap junctions contribute to treatment resistance

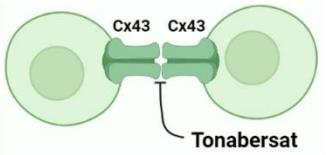

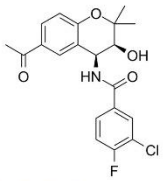

Tonabersat:

- Clinical trials regarding the prophylaxis of migraine
- Inhibits gap junction-mediated processes
- Exact mechanism not well understood

Aim:

Investigate the most potent combination of fractionated RT, TMZ chemotherapy and/or Tonabersat

Hypothesis:

Inhibition of Cx43 → increased survival rate + significantly reduced tumour volume

METHODS

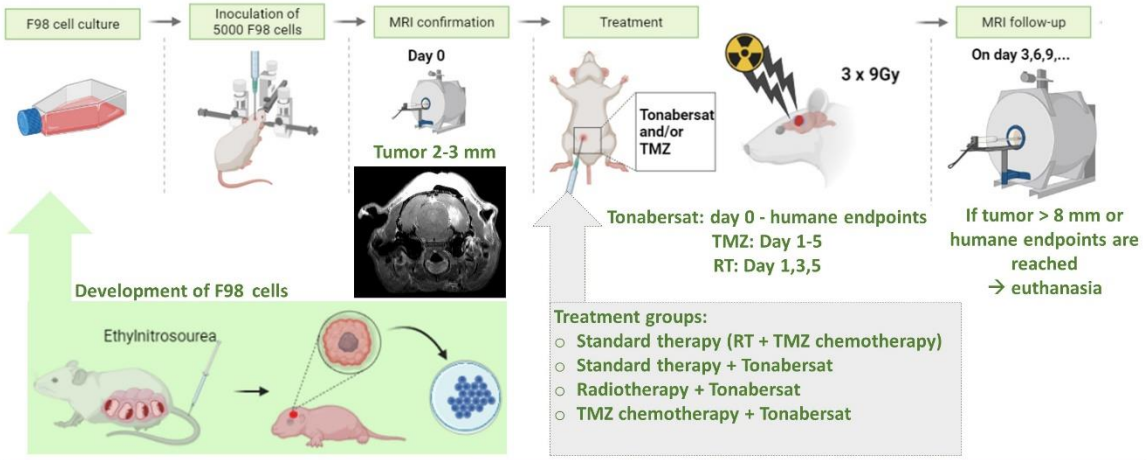

Treatment groups:

- Standard therapy (RT + TMZ chemotherapy)
- Standard therapy + Tonabersat
- Radiotherapy + Tonabersat
- TMZ chemotherapy + Tonabersat

PRELIMINARY RESULTS

	DAY 3	DAY 9	DAY 12
Standard therapy	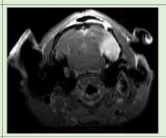	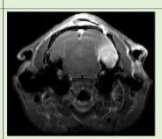	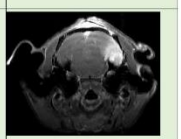
Standard therapy + Tonabersat	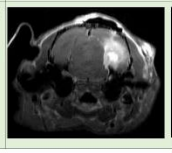	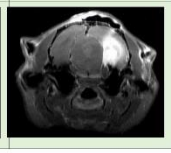	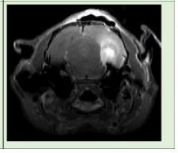

Treatment group: standard therapy

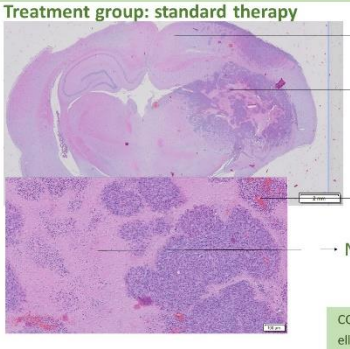

CONTACT
ellen.ketelaere@ugent.be

Addendum

Name	Group	D0	D3	D6	D9	D12	D15	D18	D21	D24	D27	D30
R2_B2_L1R0	ST control	12.7158	26.2968	31.1802	30.3876	36.2676	57.4452	94.4562				
R2_B7_L0R1	ST control	14.2998	21.9678	23.9616	24.3936	23.6268	25.0878	24.6066	64.3692	128.4462		
R2_B9_L1R0	ST control	11.4336	30.0936	31.3608	42.0492	100.23						
R3_B1_L0R0	ST control	10.1262	24.5658	25.5618	29.4816	27.1872	79.218	233.469				
Opt2_B4_L0R0	ST control	21.087	49.131	52.854	56.8158	64.149	88.1358	110.8254	184.3788	296.5812		
Opt3_B2_L0R1	ST control	27.75	51.2292	61.4136	53.304	46.6152	61.6098	121.242	158.4738	225.8484		
R3_B1_L1R0	ST control	25.464	38.8326	33.0828	49.1394	40.2132	40.2624	45.6354	55.206	195.5022		
R1_B1_L1R0	TMZ + T	14.3406	38.343	99.8544	158.091							
R1_B2_L1R0	TMZ + T	6.15	8.991	50.4132	111.1392	141.1284	205.947					
R2_B1_L1R0	TMZ + T	38.2524	73.6476	103.8396	142.9578	248.8134						
R2_B8_L0R0	TMZ + T	8.3796	19.3554	36.9294	70.821	106.7148	207.768					
R3_B1_L0R1	TMZ + T	14.4636	43.3008	71.8992	104.1498							
R3_B8_L1R0	TMZ + T	16.8318	34.962	54.3006	94.0644	172.5942						
R1_B2_L0R1	RT + T	6.2724	20.874	27.4644	32.0778	29.6292	28.4766	32.1846	48.249	66.9264	102.0504	159.7002
R2_B1_L0R1	RT + T	18.9876	42.6384	46.7628	45.6366	44.8176	53.001	62.9898	120.6864	220.8834		
R2_B2_L0R0	RT + T	28.7634	45.2184	53.5488	51.4338	74.4156	52.2012	69.8502	92.8788	134.9706		
R3_B2_L1R0	RT + T	14.0382	31.9482	44.3952	44.5332	44.8674	56.4318	77.9094	186.3144			
R3_B6_L1R0	RT + T	29.1798	48.5106	52.1364	68.2404	72.5208	55.452	84.3216	157.1352	230.2758		
R3_B3_L0R1	RT + T	8.9994	23.61	27.9462	24.5898	28.9992	32.8788	31.9644	45.7584	87.7674	137.103	
R3_B3_L1R0	RT + T	10.3308	22.197	30.7224	21.666	31.5234	23.1282	38.5386	37.7136	53.6556	84.3708	
R1_B2_L1R1	ST + T	7.236	18.0564	25.9782	24.729	28.4856	26.346	27.7752	52.3404	75.8442	192.9294	
R2_B2_L0R1	ST + T	15.1662	31.2456	34.8636	39.8856	59.4696	49.8744	65.277	101.7486	160.566		337.3974
R2_B3_L0R1	ST + T	54.1452	64.8024	68.184	65.1204	71.106	71.6628	109.2384	125.0238	187.2042	261.1458	
R2_B4_L0R0	ST + T	11.907	27.6198	29.196	31.6464	39.9684	43.9368	66.6888	93.5004	186.1194	294.4746	336.3936

R2_B4_L1R0	ST + T	43.7814	70.9764	81.936	56.1054	51.4416	52.797	77.6646	89.727	133.1826	224.1678	
R3_B6_L0R1	ST + T	17.7708	40.4988	51.3114	56.3256	51.867	48.7716	62.1888	109.5798	155.2152		
R3_B8_L0R1	ST + T	12.0618	28.8942	39.8856	29.2692	39.8934	42.246	61.6668	117.1752	187.695		

Table A1: Overview of non-log-transformed GB volumes (mm^3) used for analysis. GB volume (mm^3) was measured on CE T1w images per animal per time-point. Animals Opt2_B4_L0R0 and Opt3_B2_L0R1 are control animals from a previous experiment. Abbreviations: standard therapy (ST), Temozolomide (TMZ), fractionated radiotherapy (RT), Tonabersat (T), day (D).

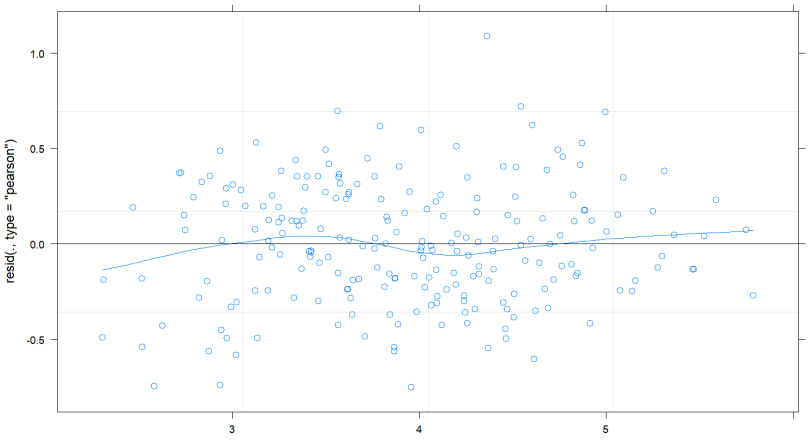

Figure A1: Residual plot indicates linearity. Results lie symmetrically in comparison to the straight line, indicating a good model.

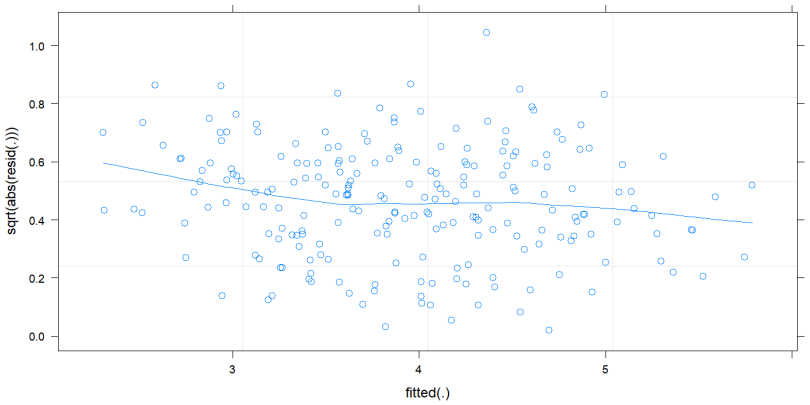

Figure A2: Homoscedasticity plot indicates a good variance between the values. No trend is observed.

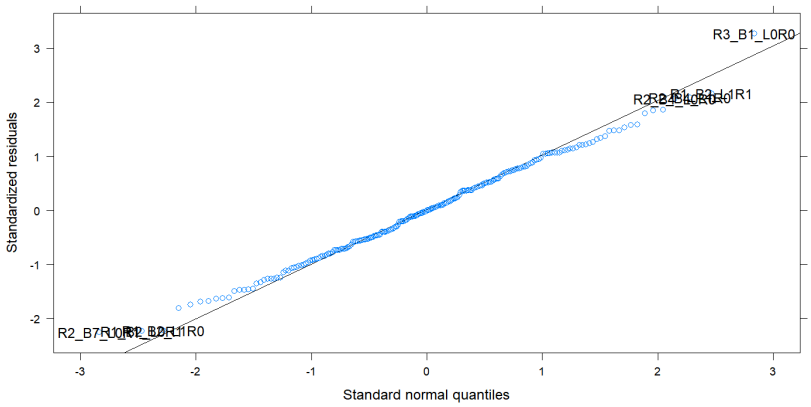

Figure A3: QQ plot. Almost all log-transformed values are laying on the straight line, indicating normality.

	ST control	TMZ + T	RT + T	ST + T
	Geometric mean GB volume (mm^3) + SD	Geometric mean GB volume (mm^3) + SD	Geometric mean GB volume (mm^3) + SD	Geometric mean GB volume (mm^3) + SD
D0	16.36013 (SD: 2.697610)	13.79183 (SD: 4.672950)	14.43295 (SD: 3.526008)	18.20986 (SD: 6.868913)
D3	32.90209 (SD: 4.512160)	30.10171 (SD: 9.096909)	31.77287 (SD: 4.454821)	36.35081 (SD: 7.573589)
D6	34.99818 (SD: 5.409859)	64.99240 (SD: 11.198982)	38.97721 (SD: 4.318177)	43.65865 (SD: 7.934085)
D9	38.98060 (SD: 4.854198)	109.69951 (SD: 13.100064)	38.34581 (SD: 6.186373)	40.79415 (SD: 5.974119)
D12	43.19980 (SD: 10.018366)	159.47212 (SD: 30.314987)	43.48312 (SD: 7.362756)	47.07682 (SD: 5.340156)
D15	54.05970 (SD: 9.604146)	206.85550 (SD: 0.910500)	40.77760 (SD: 5.408013)	46.21189 (SD: 5.130541)
D18	83.24361 (SD: 29.944637)		52.81285 (SD: 8.406158)	62.98857 (SD: 9.116620)
D21	100.94463 (SD: 32.711766)		83.08209 (SD: 22.186993)	95.36305 (SD: 9.021452)
D24	202.51555 (SD: 34.878975)		113.72765 (SD: 31.567458)	149.20667 (SD: 15.311884)
D27			105.68612 (SD: 15.495408)	240.14615 (SD: 22.061453)
D30			159.70020	336.89513 (SD: 0.501900)

Table A2: Overview of the geometric mean tumour volume (mm^3) per time-point per treatment group with according SD. This data was used to create figure 11A. From day 18 onwards a steeper increase can be observed in geometric mean GB volume (numbers in red) for the ST control group, RT + T group and ST + T group. Abbreviations: standard therapy (ST), Temozolomide (TMZ), fractionated radiotherapy (RT), Tonabersat (T), standard deviation (SD), day (D).

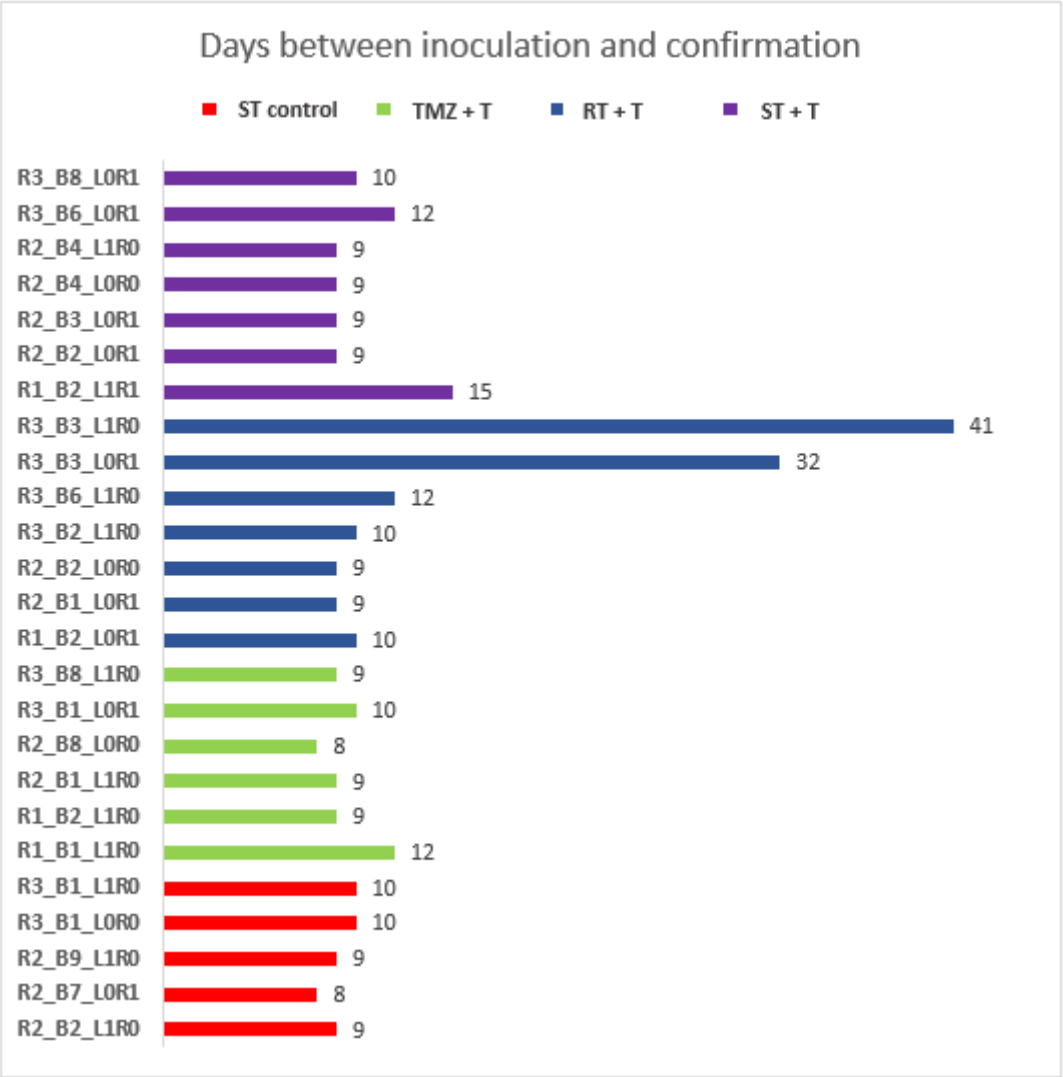

Figure A4: Overview of days between inoculation and confirmation (=d0) per animal used in this experiment. Abbreviations: standard therapy (ST), Temozolomide (TMZ), fractionated radiotherapy (RT), Tonabersat (T).

Animal	Treatment group	Weight inoculation	Weight on day of euthanasia	Day of euthanasia	Cause of euthanasia
R1_B1_L1R0	TMZ + T	139 g	117 g	D9	Clinical signs (no movement, absence of grooming, hunched back posture)
R1_B2_L1R1	ST + T	139,5 g	152 g	D27	Pathological changes observed on brain MRI
R1_B2_L0R1	RT + T	137 g	145 g	D30	Pathological changes observed on brain MRI
R1_B2_L1R0	TMZ + T	140 g	138 g	D15	Pathological changes observed on brain MRI
R2_B1_L1R0	TMZ + T	145 g	142 g	D12	Pathological changes observed on brain MRI
R2_B1_L0R1	RT + T	146 g	150 g	D27	Pathological changes observed on brain MRI (on day 24)
R2_B2_L0R0	RT + T	141 g	139 g	D25	Clinical signs (reduced activity, absence of grooming, porphyrin)
R2_B2_L0R1	ST + T	145 g	149 g	D25	Clinical signs (reduced activity, porphyrin)
R2_B2_L1R0	ST	151 g	124 g	D18	Clinical signs (reduced activity, porphyrin, tilted head)
R2_B3_L0R1	ST + T	144 g	152 g	D30	Pathological changes observed on brain MRI, clinical signs (reduced activity)
R2_B4_L1R0	ST + T	155 g	174 g	D30	Pathological changes observed on brain MRI
R2_B4_L0R0	ST + T	145 g	147 g	D27	Pathological changes observed on brain MRI, clinical signs (reduced activity, absence of grooming)
R2_B7_L0R1	ST	142 g	137 g	D24	Pathological changes observed on brain MRI, tumour metastasises through ventricle, clinical signs (reduced activity, absence of grooming, porphyrin)
R2_B8_L0R0	TMZ + T	148 g	139 g	D15	Pathological changes observed on brain MRI
R2_B9_L1R0	ST	147 g	138 g	D13	Clinical signs (reduced activity, biting)

R3_B1_L0R1	TMZ + T	148 g	144 g	D9	Pathological changes observed on brain MRI, midline shift
R3_B1_L1R0	ST	156 g	158 g	D24	Pathological changes observed on brain MRI, tumour metastasises through ventricle, clinical signs (squeaks, fearful)
R3_B1_L0R0	ST	152 g	119 g	D18	Tumour metastasises through ventricle, clinical signs (reduced activity, balance problems), weight loss
R3_B2_L1R0	RT + T	150 g	156 g	D21	Pathological changes observed on brain MRI, epilepsy attack, clinical signs (panic, squeaks)
R3_B3_L1R0	RT + T	166 g	179 g	D27	Pathological changes observed on brain MRI, clinical signs (reduced activity, absence of grooming)
R3_B3_L0R1	RT + T	149 g	157g	D27	Pathological changes observed on brain MRI, clinical signs (reduced activity, absence of grooming, porphyrin)
R3_B6_L1R0	RT + T	160 g	134 g	D24	Pathological changes observed on brain MRI, clinical signs (reduced activity, porphyrin)
R3_B6_L0R1	ST + T	153 g	175 g	D24	Pathological changes observed on brain MRI
R3_B8_L1R0	TMZ + T	154 g	150 g	D12	Pathological changes observed on brain MRI
R3_B8_L0R1	ST + T	158 g	154 g	D24	Pathological changes observed on brain MRI, clinical signs (porphyrin)

Table A3: Overview of cause of euthanasia for each animal used in the analysis. Abbreviations: Temolozomide (TMZ), fractionated radiotherapy (RT), standard therapy (ST), Tonabersat (T), day (D).